ABSTRACT

INITIAL HERTZIAN CHARACTERIZATION OF THE HUMAN TOOTH AS A DAMAGE TOLERANT BIO-CERAMIC/BIO-COMPOSITE BI-LAYER

by
Ivory Camille Kilpatrick

The objective of this thesis was to investigate the Hertzian Contact response of human teeth and how the response behavior is related to that of model ceramic bi-layers (high modulus brittle ceramics on compliant substrates). Hertzian Contact is a blunt indentation method, which uses a hard spherical indenter to apply a normal compressive load. Clinical variables of masticatory (occlusal) force and cuspal curvature identify closely with the independent Hertzian variables of contact load and sphere radius [1]. This method offers insight into the role of microstructure and microstructure-sensitive mechanical properties. It was hypothesized that tooth damage modes and patterns observed would mimic those seen in comparable dental ceramic bi-layer structures, with the same dependence on coating thickness.

Under Hertzian Contact testing teeth exhibited both classic ceramic surface ring cracking as well as quasi-plastic behavior of heterogeneous ceramics in the vicinity of the indenter. Radial cracking was seen beneath the indenter originating at the dento-enamel junction and extending upward toward the surface as seen in thin (i.e. < 1.0 mm) dental ceramic layers. The amount of ring cracking and quasi-plasticity was inversely related to loading rate, indicating visco-elastic behavior. The highly visco-elastic response found for enamel (supported by dentin) has never been identified. The mechanisms of this response are believed to lie within enamel microstructure and nano-structure.

At a low loading rate, the amount of surface indentation strain was inversely related to enamel thickness. At a high loading rate, the amount of surface indentation strain was either unrelated to or modestly related to enamel thickness depending upon the load applied. At the high loading rate, enamel exhibited elastic behavior until higher loads induced radial and ring cracks with little quasi-plastic response.

These findings infer that teeth accommodate and tolerate damage better at higher load rates due to increased elastic behavior. It appears that at higher loading rates enamel microstructure and nano-structure are better able to influence the response to loading, which results in the observance of elastic behavior and a diminishing influence of enamel thickness. Analysis of the tooth's response to Hertzian contact testing has allowed for investigation of and further insight into the microstructure-sensitive properties providing teeth with their damage tolerance.

INITIAL HERTZIAN CHARACTERIZATION OF THE HUMAN TOOTH AS A DAMAGE TOLERANT BIO-CERAMIC/BIO-COMPOSTIE BI-LAYER

by
Ivory Camille Kilpatrick

A Thesis
Submitted to the Faculty of
New Jersey Institute of Technology
In Partial Fulfillment of the Requirements for the Degree of
Master of Science in Biomedical Engineering

Department of Biomedical Engineering

August 2001

APPROVAL PAGE

INITIAL HERTZIAN CHARACTERIZATION OF THE HUMAN TOOTH AS A DAMAGE TOLERANT BIO-CERAMIC/BIO-COMPOSITE BI-LAYER

Ivory Camille Kilpatrick

Dr. Van P. Thompson, Thesis Advisor — Date
Associate Dean of Research, UMNJ –Dental School

Dr. David Kristol, Committee Member — Date
Chairperson and Professor of Biomedical Engineering, NJIT

Dr. Peter Engler, Committee Member — Date
Professor of Biomedical Engineering, NJIT

BIOGRAPHICAL SKETCH

Author: Ivory Camille Kilpatrick

Degree: Master of Science

Date: August 2001

Undergraduate and Graduate Education:

- Master of Science in Biomedical Engineering,
  New Jersey Institute of Technology, Newark, NJ, 2001

- Bachelor of Science in Applied Mathematics,
  New Jersey Institute of Technology, Newark, NJ, 1999

Major: Biomedical Engineering

Presentations and Publications:

Stephen Kao and Ivory Kilpatrick,
"Characterization of the Tooth as a Damage Tolerant Bi-Layer Structure."
The 5th Annual Symposium on Materials Research sponsored by the Center for Biomaterials, Somerset, NJ, November 2000.

Ivory Kilpatrick and Mary Caron,
"Hertzian Characterization of the Tooth as a Damage Tolerant Bio-Ceramic/Bio-Composite Bi-Layer for Bio-Mimetic Design." Associated Institutes of Material Science Symposium, Piscataway, NJ, May 2001.

Psalm 23

The Lord is my Shepherd; I shall not want.
He maketh me to lie down in green pastures:
He leadeth me beside the still waters.
He restoreth my soul:
He leadeth me in the paths of righteousness for His name' sake.

Yea, though I walk through the valley of the shadow of death,
I will fear no evil: For thou art with me;
Thy rod and thy staff, they comfort me.
Thou preparest a table before me in the presence of mine enemies;
Thou annointest my head with oil; My cup runneth over.

Surely goodness and mercy shall follow me all the days of my life,
and I will dwell in the House of the Lord forever.

This thesis is a blessing from the Lord.

I dedicate this work to my beloved family and devoted friends.

I dedicate my life to Christ.

ACKNOWLEDGMENT

I would like to express my deepest appreciation to Dr. Van P. Thompson, who not only served as my thesis advisor, providing valuable and countless resources, insight, and opportunities, but who also offered an endless supply of support, encouragement, and reassurance. I would also like to thank Dr. David Kristol and Dr. Peter Engler for being active and accommodating members of my thesis committee. Special thanks are given to Dr. John L. Ricci for his unfailing support and infinite wealth of technical knowledge and to Dr. Dianne E. Rekow for her guidance and inspiration.

I also wish to thank the following people for their administrative and technical assistance: Carolyn Booker, Dr. Rufus Caine, Elizabeth Clark, Zeena Charion, Dr. Didier Guillaume, and Dr. Allyn Luke. I extend my deep appreciation to my peers at NJIT and the UMDNJ Dental School for their support and assistance. I would like to thank the National Institute of Dental and Craniofacial Research (NIDCR) for partial funding of this work with NIDCR Grant # DE10976.

I am forever indebted to my mother and father for their undying support and guidance, shed tears, and midnight prayers. To my sister, I owe thanks for her zeal for life. To my grandparents, I owe thanks for unfailing advice and unwavering faith. To my aunts, uncles, and cousins, thank you for helping me see the bigger picture in life and for showing me the strength of family and the power of love. To my friends, thank you for the shoulder to cry on, the ear to listen, and the arms to fall into. I love you all.

TABLE OF CONTENTS

Chapter	Page
1 INTRODUCTION	1
1.1 Problem Statement	1
1.2 Research Questions	2
1.3 Study Objectives	2
1.4 Background	2
2 REVIEW OF THE LITERATURE	6
2.1 The Human Tooth	6
2.1.1 Structure	6
2.1.2 Anatomy	8
2.1.3 Microstructure	9
2.1.4 Micro-Structural Sensitive Mechanical Properties	18
2.1.5 Mechanical Properties	20
2.1.6 Functional Loading	21
2.2 Hertzian Contact	22
2.2.1 Theory	23
2.2.2 Hertzian Characterization of Layer Structures	24
2.2.3 Hertzian Characterization of Dental Layer Structures	28
2.2.4 Proposed Hertzian Characterization of the Tooth as a Bi-Layer	30
3 MATERIALS AND METHODS	33
3.1 Study Hypothesis	33
3.2 Study Design	34

TABLE OF CONTENTS
(Continued)

Chapter **Page**

3 MATERIALS AND METHODS 33

3.3 Experimental Procedures 35

3.3.1 Sampling of Teeth 35

3.3.2 Initial Processing of Teeth 35

3.3.3 Specimen Preparation for Hertzian Contact Testing 36

3.3.4 Pre-Test Processing of Specimens 39

3.3.5 Hertzian Contact Testing of Specimens 39

3.3.6 Light Microscopy: Initial Visualization of Contact Area 41

3.3.7 Post-Test Processing 41

3.3.8 Light Microscopy: Visualization of Surface Damage 43

3.3.9 Specimen Preparation for Investigation of Sub-Surface Damage 43

3.3.10 Specimen Processing 44

3.3.11 Light Microscopy: Visualization of Surface and Sub-Surface Damage. 45

3.3.12 Specimen Processing 45

3.3.13 SEM: Enhanced Visualization of Surface and Sub-Surface Damage 46

3.4 Data Collection 46

3.4.1 Qualitative Data 46

3.4.2 Quantitative Data 47

3.4.3 Statistical Data 47

3.5 Data Analysis 47

TABLE OF CONTENTS
(Continued)

Chapter **Page**

4 RESULTS 48

4.1 Qualitative Results 49

4.2 Quantitative Results 54

4.2.1 Among Groups 55

4.2.2 Within Groups 59

5 DISCUSSION 67

6 CONCLUSIONS AND FUTURE WORK 80

APPENDIX ADDITIONAL DATA AND FIGURES 83

REFERENCES 89

LIST OF TABLES

Table		Page
2.1	Composition of Hard Tissues by Volume (%), Weight (%) in brackets	9
2.2	Mechanical Properties of Enamel and Dentin	21
4.1	Mean values of independent and dependent variables among groups	55
4.2	Data set for specimens tested to a load of 50 N at a load rate of 18 N/min	60
4.3	Data set for specimens tested to a load of 100 N at a load rate of 144 N/min	60
4.4	Data set for specimens tested to a load of 150 N at a rate of 144 N/min	60
A.1	Raw data for all specimens successfully tested	83
A.2	Data set for specimens tested to a load of 75 N at a rate of 18 N/min	84

LIST OF FIGURES

Figure		Page
2.1	Cross-section of a molar tooth in situ	7
2.2	Diagram illustrating the varying crystalline orientation within the head and tail region of an enamel rod	10
2.3	Diagram of arrangement of enamel rods relative to surrounding rods	10
2.4	Diagram depicting the fish-scale appearance of enamel in an de-mineralized or etched section	11
2.5	Diagram illustrating the difference in direction between rows of enamel rods	12
2.6	Diagram illustrating the intertwining (i.e. decussation) of layers or groups of enamel rods	12
2.7	Diagram illustrating the crossing of groups of enamel rods	13
2.8	Image of gnarled enamel in the vicinity of the DEJ	14
2.9	Diagram illustrating crack propagation around the rod sheaths of enamel rods	14
2.10	Diagram depicting appearance of enamel rods in different sections of the tooth	15
2.11	Image illustrating the scalloped appearance of the DEJ	16
2.12	Series of diagrams depicting the complexity of the microstructure of the DEJ	17
2.13	Diagram illustrating the bonded interface technique for Hertzian Contact testing	24
2.14	Diagram illustrating the damage modes and patterns observed in monolithic materials	26
2.15	Damage modes generally produced in bi-layer structures relative to the thickness of the coating layer	28
4.1	Light microscopy image of the enamel surface of a specimen tested to a load of 75 N at a load rate of 18 N/min	50
4.2	Light microscopy image of the enamel surface of a specimen tested to a load of 150 N at a load rate of 144 N/min	51

LIST OF FIGURES
(Continued)

Figure **Page**

4.3 SEM image of the enamel in an angulated cross –sectional view of a specimen tested to a load of 100 N at a load rate of 144 N/min 52

4.4 SEM image of the enamel in an angulated cross –sectional view of a specimen tested to a load of 75 N at a load rate of 18 N/min 52

4.5 SEM image of the enamel in an angulated cross –sectional view of a specimen tested to a load of 75 N at a load rate of 18 N/min 53

4.6 SEM image of the enamel in an angulated cross –sectional view of a specimen tested to a load of 75 N at a load rate of 18 N/min 54

4.7 Plot of Contact Radius vs. Load Rate, Independent of Applied Load among groups 56

4.8 Plot of Indentation Stress vs. Applied Load among groups 57

4.9 Plot of Indentation Stress vs. Load Rate, Independent of Applied Load among groups 57

4.10 Plot of Indentation Strain vs. Load Rate, Independent of Applied Load among groups 58

4.11 Plot of Contact Radius vs. Enamel Thickness for an Applied Load of 50 N at a Load Rate of 18 N/min 61

4.12 Plot of Indentation Stress vs. Enamel Thickness for an Applied Load of 50 N at a Load Rate of 18 N/min 62

4.13 Plot of Indentation Strain vs. Enamel Thickness for an Applied Load of 50 N at a Load Rate of 18 N/min 62

4.14 Plot of Contact Radius vs. Enamel Thickness for an Applied Load of 100 N at a Load Rate of 144 N/min 63

4.15 Plot of Contact Radius vs. Enamel Thickness for an Applied Load of 150 N at a Load Rate of 144 N/min 64

4.16 Plot of Indentation Stress vs. Enamel Thickness for an Applied Load of 150 N at a Load Rate of 144 N/min 65

LIST OF FIGURES
(Continued)

Figure **Page**

4.17 Plot of Indentation Strain vs. Enamel Thickness for an Applied Load of 150 N at a Load Rate of 144 N/min 65

5.1 SEM image of the enamel surface of a specimen tested to a load of 50 N at a load rate of 18 N/min 73

5.2 Light microscopy image of the enamel surface of a specimen tested to a load of at a load rate of 18 N/min 77

A.1 Plot of Relative Elastic Modulus vs. Applied Load among groups 83

A.2 Plot of Relative Elastic Modulus vs. Load Rate, Independent of Applied Load among groups 84

A.3 Plot of Relative Elastic Modulus vs. Enamel Thickness for an Applied Load of 50 N at a Load Rate of 18 N/min 84

A.4 Plot of Contact Radius vs. Enamel Thickness for an Applied Load of 75 N at a Load Rate of 18 N/min 85

A.5 Plot of Indentation Stress vs. Enamel Thickness for an Applied Load of 75 N at a Load Rate of 18 N/min 85

A.6 Plot of Indentation Strain vs. Enamel Thickness for an Applied Load of 75 N at a Load Rate of 18 N/min 86

A.7 Plot of Relative Elastic Modulus vs. Enamel Thickness for an Applied Load of 75 N at a Load Rate of 18 N/min 86

A.8 Plot of Indentation Stress vs. Enamel Thickness for an Applied Load of 100 N at a Load Rate of 144 N/min 87

A.9 Plot of Indentation Strain vs. Enamel Thickness for an Applied Load of 100 N at a Load Rate of 144 N/min 87

A.10 Plot of Relative Elastic Modulus vs. Enamel Thickness for an Applied Load of 100 N at a Load Rate of 144 N/min 88

A.11 Plot of Relative Elastic Modulus vs. Enamel Thickness for an Applied Load of 150 N at a Load Rate of 144 N/min 88

CHAPTER 1

INTRODUCTION

This chapter provides insight into the nature and scope of Hertzian characterization of the tooth as a bi-layer structure. It will begin with a statement of the problem, research questions, and the study objectives of this thesis. It will conclude by offering background into the clinical relevance of the problem and study objectives.

1.1 Problem Statement

- There has been limited characterization of the human tooth as a bi-layer structure.
- The relationship between and the role of microstructure and microstructure-sensitive mechanical properties operating during functional loading have not been investigated for the tooth. Hertzian Contact testing provides clinically relevant insight into these relationships and roles.
- Dental layer structures, composed of ceramic coating layers and polymer/ composite substrates, have been characterized using Hertzian Contact.
- The bi-layer structure of the tooth, composed of enamel (a bio-ceramic coating layer) and dentin (a bio-composite substrate), that dental layer structures are designed to mimic, has not been characterized using Hertzian Contact. This limits the ability for comparisons between the response of natural tooth structure and restorative dental layer structures to forces relative to those applied during functional loading.

1.2 Research Questions

- Does the tooth, as a bi-layered bio-ceramic/bio-composite, have the same response to Hertzian Contact testing as dental layer structures of a ceramic coating supported by a polymer substrate?
- Do independent Hertzian Contact variables of coating thickness and contact load play the same role in determination of the damage produced in tooth structure as they do in dental layer structures?

1.3 Study Objectives

- Hertzian characterization of the tooth as a bio-ceramic/bio-composite bi-layer permitting comparison of the tooth's response to that of dental layer structures.
- Investigation of the strength of the relationship between thickness and load to the damage produced.
- Investigation of the relationship between microstructure and mechanical response to loading as evident by damage observed.

1.4 Background

The tooth is a resilient and damage tolerant bi-layer structure composed of enamel and dentin. This bi-layer corresponds to a hard (high elastic modulus), anisotropic, and protective brittle material bonded to a soft (low elastic modulus), supportive, and tough substrate. The bond between these two very different layers is known as the dentino-enamel junction or DEJ. The DEJ is a thin layer, which serves as a transition zone with

properties that range from that of enamel to that of dentin. It is believed to play a critical role in the transfer of stress across the layers of the tooth. [1]

Teeth are uniquely able to withstand masticatory forces greater than 200 N over contact areas as small as 0.5 mm^2 for more than 10^7 cycles of contacts between opposing cusps of characteristic radii of 2 to 4 mm for durations averaging 100 ms, with little incidence of total failure or evidence of damage (i.e. cracks). Dental crown restorations are designed to restore tooth function and esthetics. They are expected to tolerate loads of greater than 100 N over contact areas of 0.55 mm^2 for more than 10^6 cycles without failure. However, current all ceramic crowns on molar teeth have high failure rates of 1-5% per year. [1, 2]

Dental crown restorations essentially consist of a veneer material and restorative core material. The veneer is bonded to the restorative core by luting cement. The restorative core generally has the same bulk properties as dentin (i.e. low elastic modulus and toughness). The veneer material generally has the same general bulk properties as enamel (i.e. high elastic modulus and brittleness). The luting cement bond layer is generally thicker than the DEJ, due to clinical limitations. It does not have the same range of properties as does the DEJ. However, like the DEJ it serves to prevent de-lamination of the outer veneer from the inner restorative core or dentin upon loading. [1] Conceptually, this tripartite system structurally corresponds to tooth structure (i.e. enamel, dentin, and the DEJ). However, the performance of the natural tooth versus dental crown restorations differs significantly. [2]

The differences in damage tolerance and lifetimes indicate that it is more than the bi-layer structure and the bulk properties of enamel and dentin, which gives the tooth

unique tolerance. The relationship between the microstructure and microstructure-sensitive properties must be of relevance. The mechanism of stress transfer between and within the microstructure of each layer (i.e. enamel and dentin) must also be critical to the tooth's mechanical integrity and remarkable performance. The micro-mechanics of how enamel and dentin are able to absorb high loads and cycles under functional loading as a bi-layered structure has yet to be studied in any fundamental way. There is a need for characterization of the tooth as a bi-layer structure by a testing methodology that offers insight into the tooth's response, accommodation, and tolerance of functional load on the micro-structural level.

Hertzian Contact or Indentation testing, coupled with macroscopic and microscopic visualization of damage, is a methodology that will allow for the investigation of the damage tolerance of the tooth and the underlying micro-structural and micro-mechanical interactions and events. Hertzian Contact is a blunt indentation method, which uses a hard spherical indenter for the application of normal compressive loads [3]. Clinical variables of masticatory (occlusal) force and cuspal curvature identify closely with the independent Hertzian variables of contact load and sphere radius [1]. Therefore, it simulates functional-loading conditions (i.e. occlusion resulting from mastication) [4] much more compellingly than conventional mechanical tests. In addition to its clinical relevance, Hertzian indentation provides more insight into the role of integration of microstructure and micro-mechanical properties because it operates on the macro-structural scale of the material(s) tested [3].

Hertzian Contact has been used for the characterization of dental layer structures for crown restorations that correspond to enamel support by dentin [5]. Hertzian

characterization of tooth as a bi-layer structure will allow for comparison of the response of the natural tooth and dental restorations, designed to replace tooth structure, to loading mechanisms comparable to functional loading. Elucidation of the role of microstructure and micro-mechanical properties of the tooth structure would serve as the basis for the design of more bio-mimetic dental ceramic or resin based composite crowns [1]. The result being, dental crown restorations that both esthetically replace tooth structure and effectively restore tooth function with service lives approaching those of natural teeth.

CHAPTER 2

REVIEW OF THE LITERATURE

This chapter will present a review of the literature of the human tooth and Hertzian contact. It will provide background into the structure, function, and mechanical properties of the tooth. It will present the theory of Hertzian Contact and review Hertzian characterization of layer structures and dental layer structures. It will conclude with the rationale and theoretical framework for the proposed Hertzian characterization of the tooth.

2.1 The Human Tooth

2.1.1 Structure

The tooth can be viewed as consisting of a crown and a root (refer to Figure 2.1). The crown is the portion that is visible within the oral cavity (i.e. the mouth). The root is the portion that lies beneath the surface of supporting tissues and bone. The junction between the crown and the root is known as the cervical margin. [6]

The crown of the tooth is comprised of an outer layer of enamel and an inner core of dentin (refer to Figure 2.1). Enamel is a highly mineralized, hard, inert, a-cellular substance. Dentin is a less mineralized, resilient, vital, hard connective tissue. Enamel is bonded to dentin by a thin layer known as the dentino-enamel junction (DEJ). The dentino-enamel junction has a gradient of properties ranging from those of enamel to those of dentin. It is thought of as a transition zone. Enamel and dentin provide the tooth unique hardness and resilience properties. Embedded within the dentin core of the crown

is the pulp. The pulp is a filament of soft connective tissue that formed and supports dentin. It contains cells, nerves, and blood vessels that enter the tooth via an opening at the apex of the root. [6]

The root of the tooth is primarily composed of dentin, covered by a layer of cementum, a connective tissue (refer to Figure 2.1). The root is embedded in the underlying and supporting alveolar bone, attached by a layer of fibrous connective tissue known as the periodontal ligament (PDL) or membrane. This attachment provides the flexibility needed to withstand masticatory forces. [6]

Figure 2.1 Cross-section of a molar tooth in situ. (Reproduced from Eisenmann, D.R., *Enamel Structure, in Oral Histology: Development, Structure, and Function.* 1989, C.V. Mosby Company: St. Louis. p. 213-28.)

2.1.2 Anatomy

2.1.2.1 Enamel. The shell of enamel that covers the crown of the tooth varies in thickness according to tooth type and location; at a maximum, thickness is 2.5 to 3 mm [7]. On any class of tooth (i.e. canine, incisor, pre-molar, or molar), enamel is thickest at the incisal or occlusal surface (i.e. load bearing surface). Thickness continually decreases until the cervical margin (i.e. the cemento-enamel junction) is reached, at which point the cementum covered root begins. [7, 8]

Enamel is the most highly mineralized (i.e. hardest) tissue found in the human body; it is approximately 96% inorganic material and the balance is organic material. The mineralized (inorganic) matrix or material is comprised primarily of hydroxyapatite crystallites. These crystals are of large size and high crystallinity. [6]

The hydroxyapatite crystallites within the enamel are preferentially packed. The difference in the orientations of the crystallites and their alignment create enamel rods (prisms), the micro-structural unit of enamel, and the interrod substance. The interrod substance is comprised primarily of apatite crystallites aligned and oriented in directions different from those found within the rods. The bulk of the organic material is found enveloping individual hydroxyapatite crystallites and surrounding individual enamel rods/interrods in a protein rich rod sheath. Thus, it is the mineralized (inorganic) matrix or material that contributes most to the microstructure of enamel. [6]

2.1.2.2 Dentin. Dentin is also a highly mineralized tissue; it is approximately 70% inorganic material and the balance organic material. The mineralized (inorganic) matrix or material is comprised primarily of hydroxyapatite crystallites, as is the inorganic matrix of enamel. The organic matrix or material is comprised primarily of fibrous

protein collagen. The micro-structural units of dentin are tubules. Dentin tubules are comprised of the cytoplasmic extensions of odontoblasts, the cells that formed and maintain dentin. [6]

The relative compositions of enamel and dentin as compared to bone are given in below in Table 2.1.

Table 2.1 Composition of Hard Tissues by Volume (%), Weight (%) in brackets.

	Bone	Dentine	Enamel
Mineral	41	48	92
(density, 3000 $kg \cdot m^{-3}$)	(64)	(69)	(97)
Organic	48	29	2
(density, 1400 $kg \cdot m^{-3}$)	(31)	(20)	(1)
Water	11	23	6
(density, 1000 $kg \cdot m^{-3}$)	(5)	(11)	(2)

Source: Waters, N.E., *Some mechanical and physical properties of teeth*. Symp Soc Exp Biol, 1980. 34: p. 99-135.

2.1.3 Microstructure

2.1.3.1 Enamel. The micro-structural unit of enamel is a rod. Each enamel rod has a specific spatial relationship to a region directly cervical to it known as its interrod [8]. A transverse section of a rod and its interrod reveals a confluence of crystals in the shape of a rounded head or body section (rod) and a tail section (interrod) that has been likened to a keyhole. This is illustrated in Figure 2.2. Generally, the head or body of a rod is oriented in the incisal or occlusal direction and the tail oriented in the cervical direction. [7, 8]

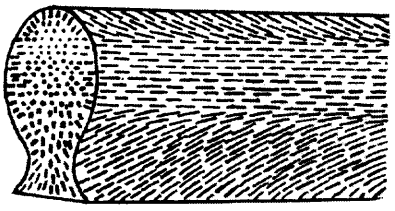

Figure 2.2 Diagram illustrating the varying crystalline orientation within the head and tail region of an enamel rod. (Reproduced from Waters, N.E., *Some mechanical and physical properties of teeth*. Symp Soc Exp Biol, 1980. 34: p. 99-135.)

The rounded head portion of each rod lies between the narrow tail (interrod) portions of two adjacent rods and below the tail or interrod of the rod above. This arrangement forms a repetitive series of densely packed interlocking rods and interrods. It results in series of four interrods surrounding the head of a rod. Only the interrod lying directly cervical to the rod will have a continuous crystalline structure with it. This results in a sharp discontinuity between the directions of crystals of the given rod and those of the other three surrounding interrods. The sharp discontinuity created by this arrangement results in the production of a rod sheath around each of the other three surrounding interrods. [8] This arrangement is illustrated in below in Figure 2.3.

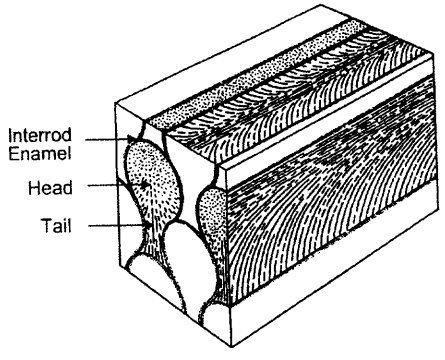

Figure 2.3 Diagram of arrangement of enamel rods relative to surrounding rods. (Reproduced from Habelitz, S., et al., *Mechanical properties of human dental enamel on the nanometer scale*. Arch Oral Biol, 2001. 46(2): p. 173-83.)

The rod sheath is a space created by the ends of the crystals comprising the head portion of the given rod and those comprising the tail or interrod portion of the surrounding rods meeting at sharp angles due to the significant degree of difference in the alignment and orientation of the opposing crystals. Rod sheaths contain most of the organic material (i.e. proteins) within enamel; the presence of this organic material within the rod sheaths is what accounts for the fish-scale appearance of enamel in a de-mineralized or etched section perpendicular to enamel rods. [8] This fish-scale appearance is illustrated below in Figure 2.4.

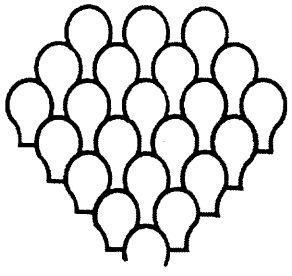

Figure 2.4 Diagram depicting the fish-scale appearance of enamel in an de-mineralized or etched section. (Reproduced from Waters, N.E., *Some mechanical and physical properties of teeth*. Symp Soc Exp Biol, 1980. 34: p. 99-135.)

The number of rods varies from approximately 5 million for a mandibular incisor to approximately 12 million for a maxillary molar [7]. The rods follow an undulating course, extending from the inner dentino-enamel junction to the outer surface of the tooth. The rods are generally aligned perpendicular to both the dentino-enamel junction and the tooth surface except for in the cervical region [9]. In the permanent (i.e. adult) dentition, enamel rods in the cervical region are oriented outward in a direction that is slightly apical.[7] Enamel rods are tapered, increasing in mean diameter slightly, from approximately 4 micrometers to 8 micrometers, as they follow an undulating course from the inner dentino-enamel junction to the outer enamel to compensate for the larger outer

surface of the crown as they create a columnar enamel microstructure.[7] Rod width averages 5 micrometers, corresponding to the diameter of the columnar ameloblasts, the formulative cells of enamel. [8]

In tangential longitudinal sections, enamel rods are arranged in roughly horizontal rows. Rod direction in one row will differ slightly from those in rows above and below it. This is illustrated in Figure 2.5. Collectively, these slight differences in rod direction will lead to decussation of rows of rods and the formation of what has been referred to as "displacement planes." [10] Enamel rods have this alternating arrangement and intertwining (decussation) of groups or layer of rods as their orientation changes from their emergence at the dentino-enamel junction to their end, 30 micrometers from the enamel surface [7]. This is illustrated Figure 2.6.

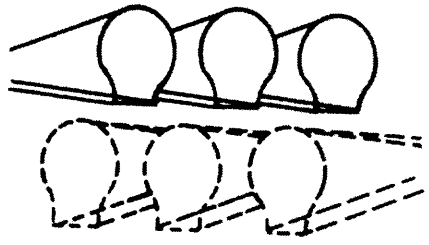

Figure 2.5 Diagram illustrating the difference in direction between rows of enamel rods. (Reproduced from Waters, N.E., *Some mechanical and physical properties of teeth.* Symp Soc Exp Biol, 1980. 34: p. 99-135.)

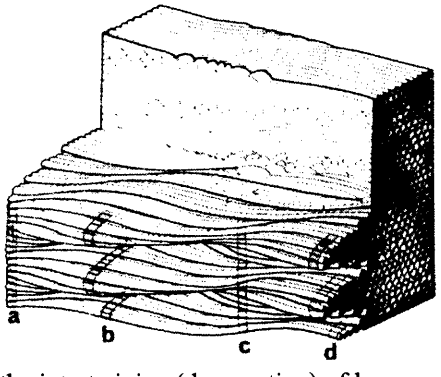

Figure 2.6 Diagram illustrating the intertwining (decussation) of layers or groups of enamel rods. (Reproduced from Osborn, J.W., *Directions and interrelationships of enamel prisms from the sides of human teeth.* J Dent Res, 1968. 47(2): p. 223-32.)

Similarly, groups of enamel rods have been observed to cross over one another in their course from the DEJ to the enamel surface, which is also referred to as decussation. [11] This crossing of groups of enamel rods is illustrated in Figure 2.7.

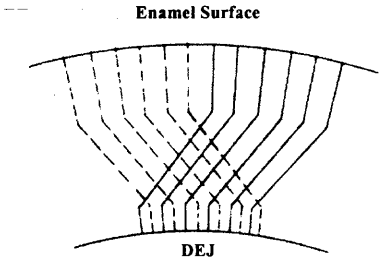

Figure 2.7 Diagram illustrating the crossing of groups of enamel rods. (Reproduced from Waters, N.E., *Some mechanical and physical properties of teeth*. Symp Soc Exp Biol, 1980. 34: p. 99-135.)

Within the initial third of the enamel, closest to the DEJ, the enamel rods follow a more undulating path known as gnarled enamel (groups of enamel rods undergoing decussation seen in longitudinal section similar to the lower third of the enamel schematic shown in Figure 2.7). This gnarling of enamel rods near the DEJ is shown is Figure 2.8. Gnarling of the enamel rods is believed to provide strength to the microstructure by offering resistance to external loads. The highly inorganic make-up of enamel rods makes crack propagation through them difficult. Given that cracks seek the path of least resistance (i.e. the weakest interface), cracks must propagate around the protein rich (i.e. organic) rod sheath surrounding enamel rods. Gnarling of enamel further limits crack propagation by making the arrangement of enamel rods and their surrounding sheaths more complex. This is illustrated in Figure 2.9. Accordingly, gnarled enamel is not subject to cleavage as is the more regularly structured enamel. The remaining two thirds of the enamel is formed by adjacent groups of less decussated enamel rods, following a less circuitous/curvy path. [6, 7]

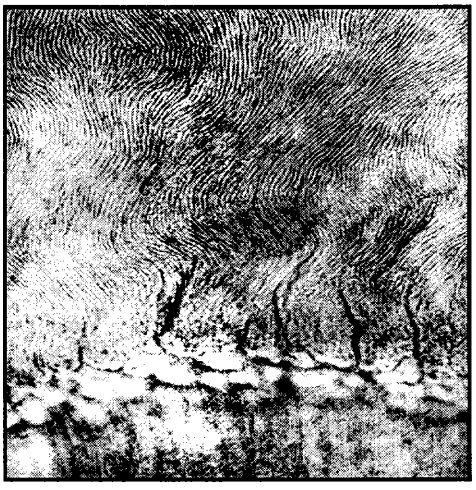

Figure 2.8 Image of gnarled enamel in the vicinity of the DEJ. Enamel Tufts are also illustrated. (Reproduced from Lundeen, T.F., Sturdevant, J.R. and Sluder, T.B. Jr, *Clinical significance of dental anatomy, histology, physiology, and occlusion*, in *The Art and Science of Operative Dentistry*, C.M. Sturdevant, Editor. 1995, Mosby: St. Louis. p. 10-57.)

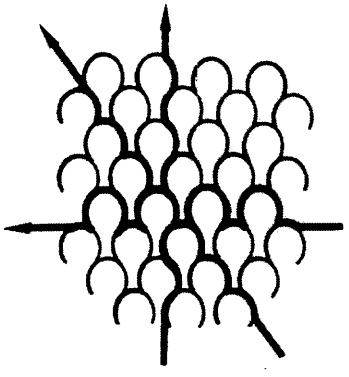

Figure 2.9 Diagram illustrating crack propagation around the rod sheaths of enamel rods. (Reproduced from Waters, N.E., *Some mechanical and physical properties of teeth*. Symp Soc Exp Biol, 1980. 34: p. 99-135.)

In tooth sections parallel to the long axis of the tooth, enamel rods appear straight. In sections perpendicular to the long axis of the tooth enamel rods appear wavy. In tangential sections (i.e. sections perpendicular to the aforementioned orientations), enamel rods appear wavy with their long axis parallel to that of the tooth.[12] Changes in the orientation of enamel rods produce optical effects, which appear as alternating zones of light and dark zones of varying widths, called Hunter-Schreger bands. [8] Since the direction of rods within enamel is variable in each tooth and between classes of teeth,

these bands are found in varying numbers in each tooth and in different areas of each class of teeth [7]. These are depicted below in Figure 2.10.

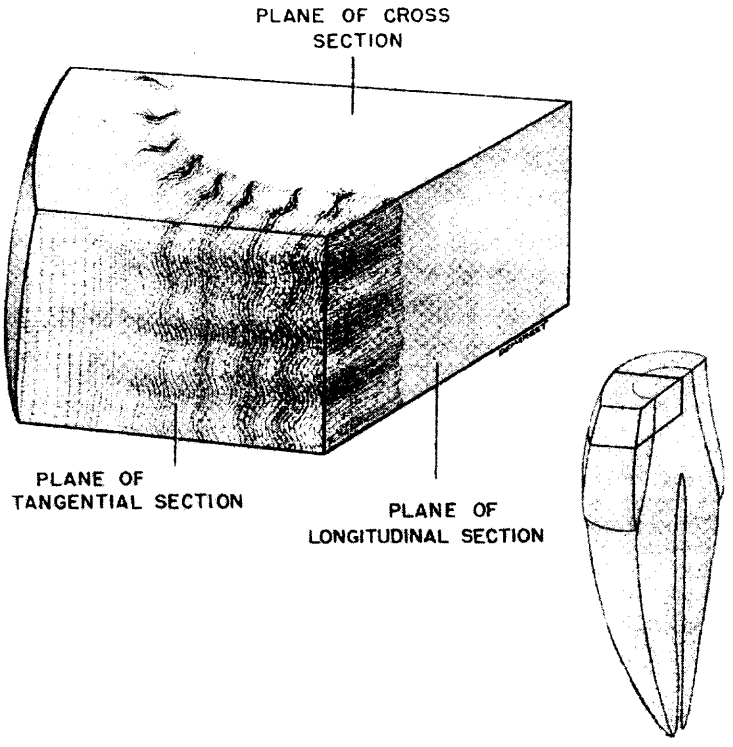

Figure 2.10 Diagram depicting appearance of enamel rods in different sections of the tooth. Hunter-Schreger bands are also illustrated. Enamel tufts are also depicted on plane of cross-section. (Reproduced from Applebaum, E., *The arrangement of enamel rods.* NY State Dental Journal, 1960. 26: p. 185-188.)

Like all other materials, enamel has imperfections that are considered characteristic structural features[13]. The most commonly observed are enamel tufts and enamel lamellae, which can be likened to geometric faults [8]. Enamel tufts originate in the dentino-enamel junction and they project into the enamel [8], between adjacent groups of enamel rods [7], for a short distance. They appear branched and they contain a high percentage of the organic material (i.e. enamel protein or organic debris) relative to the rest of the enamel. Tufts are believed to be the result of the drastic changes in the

alignment and orientation of groups of rods that radiate from the different regions of the scalloped dentino-enamel junction.[8] These are shown in Figures 2.8 and 2.10. Enamel lamellae originate in the enamel and they extend, between rod groups, towards the dentino-enamel junction and sometimes into the underlying dentin. They are thin, linear, leaf-like defects filled with organic material (i.e. enamel protein or organic debris). [7, 8]

2.1.3.2 DEJ. The DEJ is a hyper-mineralized zone that has a thickness in the range of 10 – 50 μm, conservatively [7]. Microscopically, the DEJ, appears as a well-defined scalloped or wavy border. The crests of the waves penetrate towards and into the enamel. Rounded projections of enamel fill the troughs, which appear as shallow depressions into dentin [13]. This scalloping is shown in Figure 2.11. The wavy structure of the DEJ, which provides a type of inter-digitation, is believed to contribute to the firm attachment between enamel and dentin. [7] The degree of scalloping and the size of scallops vary with location on a given tooth and among teeth. [14]

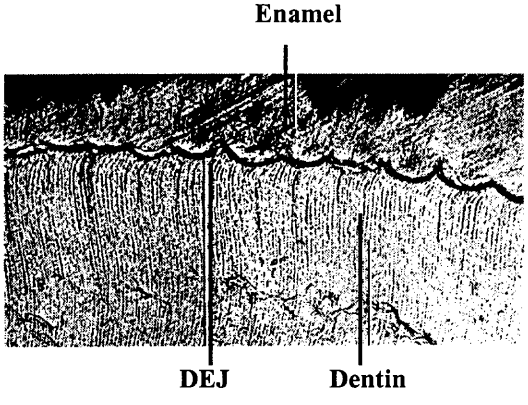

Figure 2.11 Image illustrating the scalloped appearance of the DEJ. (Reproduced from Lundeen, T.F., Sturdevant, J.R. and Sluder, T.B. Jr, *Clinical significance of dental anatomy, histology, physiology, and occlusion*, in *The Art and Science of Operative Dentistry*, C.M. Sturdevant, Editor. 1995, Mosby: St. Louis. p. 10-57.)

Recent work [15], found that these macro-scallops of the DEJ contained micro-scallops. In addition, within each micro-scallop, Type I collagen fibrils were found to extend from the dentin, coalesce into coarse fibrils, cross the DEJ, and insert into enamel. These fibrils were found to have diameters of 80-120 nm. [15] Therefore, the DEJ forms a complex interface operating on three levels: maco-scallops of varying size and degree of scalloping, micro-scallops within each scallop, and nanometer fibrils within each micro-scallop. [16] The complexity of the DEJ is illustrated below in the Figure 2.12.

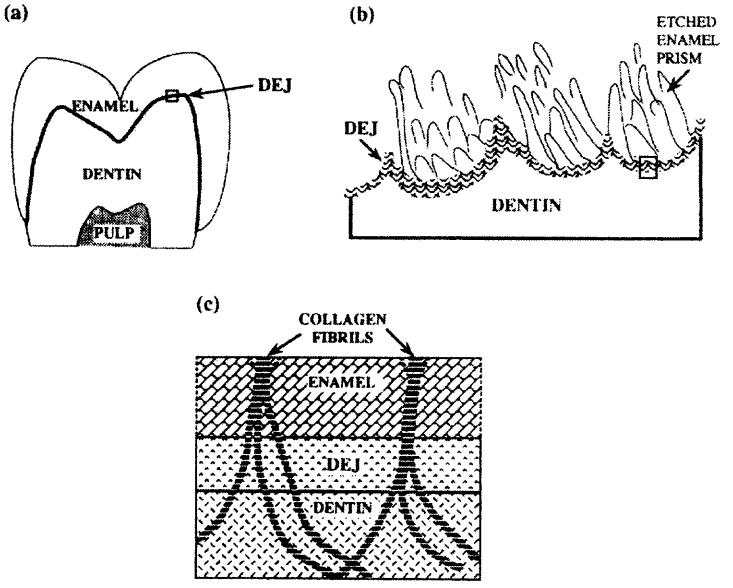

Figure 2.12 Series of diagrams depicting the complexity of the micro-structure of the DEJ. (Reproduced from Lin, C.P., W.H. Douglas, and S.L. Erlandsen, *Scanning electron microscopy of type I collagen at the dentin-enamel junction of human teeth.* J Histochem Cytochem, 1993. 41(3): p. 381-8.)

2.1.3.3 Dentin. The micro-structural unit of dentin is the dentin tubule. Dentin tubules are tube-like spaces, extending throughout the entirety of the thickness of dentin. They radiate from the dental pulp upward/outward to the DEJ or dentino-cementum interface. The alignment ant orientation of the dentin tubules indicates the path taken by the odontoblasts during dentino-genesis (i.e. the formation of dentin). The tubules are

tapered, measuring approximately 2.5 micrometers in diameter near the dental pulp, where they begin, 1.2 micrometers in the mid-portion of the dentin, and 900 nm near the dentino-enamel junction and dentino-cementum interface, where they end. [13]

2.1.4 Micro-Structural Sensitive Mechanical Properties

The tooth as previously described has a unique microstructure consisting of primarily of enamel rods, the DEJ, and dentin. The effects of these microstructures, primarily enamel rods and the DEJ, on the mechanical properties of teeth, such as hardness, fracture toughness, and elastic modulus have not been fully investigated. The hardness of teeth has been repeatedly evaluated using various micro-indentation methods [17-19]. However, in these studies, little attention was paid the influence of enamel rod orientation or proximity to the DEJ. [20]

Studies of fracture toughness and elastic modulus have employed the use of traditional flexural and tensile tests [21-23]. However, these test generally generate a single macroscopic crack and therefore do not allow for much investigation of microscopic damage or its relationship to micro-structural features of the tested structure. The use of indentation tests to assess fracture toughness and elastic modulus offers an alternative to these traditional flexural and tensile tests [24]. Indentation tests generally produce microscopic cracks and therefore do allow for investigation of macro damage and its relationship to micro-structural features of the tested material. [20] Fracture toughness [25] and elastic modulus [19, 26] of teeth have been investigated using indentation tests. However, again in these studies, the dependence of crack propagation

and mechanical properties on enamel rod orientation and the DEJ were not taken into account. [20]

An understanding of the micro-fracture and deformation and the microstructure interactions within teeth is paramount to the elucidation of their micro-structural sensitive mechanical properties. It is hypothesized that crack propagation and deformation is greatly influenced/controlled by enamel microstructure (i.e. rods) and the dentino-enamel junction (DEJ). Under this assumption, it is believed that micro-mechanical properties are influenced by enamel rod orientation and tooth-to-tooth variation. In order to better understand the micro-structural sensitive properties of teeth, an investigation of the effects of enamel rod orientation and the DEJ must be studied.[1]

Xu et al 1998 examined the effect of enamel rod orientation by propagating cracks in occlusal and axial sections of molar teeth in planes parallel and perpendicular to the occlusal surface. Using a Vickers Indentation test, a sharp contact with a diamond shaped indenter, it was shown that in the axial sections, fractures were significantly longer in directions perpendicular to the occlusal surface than parallel. In addition, those fractures propagating toward the DEJ were arrested; they did not penetrate into the underlying dentin substrate. Fracture toughness (i.e. resistance to fracture) was found to vary by a factor of three as a function of enamel rod orientation. Elastic modulus was also observed to significantly differ between occlusal and axial planes. It was concluded that cracks strongly interact with enamel rods and the DEJ. It is believed, therefore, that the mechanical properties, at least of fracture toughness and hardness, are functions of micro-structural elements and orientation. [20]

2.1.5 Mechanical Properties

Hard structures, which are resistant to wear, are traditionally brittle and offer little resistance to crack propagation (i.e. fail due to fracture). Tough materials, which offer greater resistance to crack propagation, are not very resistant to wear (i.e. fail due to fatigue). However, teeth, which are comprised of both a hard (enamel) and a tough (dentin) material, have evolved in a manner that incorporates the properties of hardness (i.e. wear resistance) and toughness (i.e. fracture resistance or crack propagation) to produce a remarkable structure that is able to function effectively, primarily as an organ of mastication, for many years. [27]

The enamel shell of the tooth, which is extremely susceptible to fracture while being approximately five time harder than its dentin substrate, functions as a hard, high-stiffness, wear resistant layer [27]. However, enamel's hardness, which is comparable to that of mild steel, also makes it brittle, having a high elastic modulus and low tensile strength; enamel is a very rigid material [7, 8]. If unsupported by an underlying more resilient substrate, enamel would fracture very easily. The highly compressive dentin substrate provides a flexible cushion for the overlying brittle enamel, preventing its total fracture and maintaining tooth integrity. Thus, the dentin core of the tooth, which has poor wear resistance while being nearly four times tougher than its enamel covering, functions as low-stiffness, stress dissipating, support layer.[7] Ranges of common mechanical properties of enamel and dentin are given in Table 2.2.

Table 2.2 Mechanical Properties of Enamel and Dentin

	Enamel	Dentin
Compressive Strength (MPa)	95-140	230-370
Young's Modulus (GPa)	9-90	11-20
Shear Strength (MPa)	90.2	36-138
Tensile Strength (MPa)	8-35	31-104
Microhardness (GPa)	3.2-4.4	0.25-0.8
K_{IC} (MPa.m ^{½})	1.3	2.8

Source: Marshall, G.W., et al., *Mechanical properties of the dentino-enamel junction: AFM studies of nanohardness, elastic modulus, and fracture.* J Biomed Mater Res, 2001. 54(1): p. 87-95.

2.1.6 Functional Loading

The response of enamel and dentin, as a bi-layer, during mastication (i.e. functional loading) is generally unknown. [28] The size of contact area and the loads delivered during normal tooth function have a significant influence on which damage mechanisms are likely to dominate intra-orally (clinically). For clinically significant data, it is necessary to determine an appropriate range for these values as a guideline for laboratory test design. [4]

Throughout their lifecycle, teeth are subjected to functional forces resulting primarily from mastication (chewing) and swallowing [4]. The highest masticatory loads are generated when the opposing cusps (with a characteristic radii of 2 to 12 mm depending upon wear between cusps of maxillary and mandibular teeth, primarily the posterior pre-molars and molars, are in contact [4]. Generally, these tooth contacts have very short durations averaging 100 milliseconds during mastication (chewing) and swallowing [29].

In humans, average maximum biting forces are reported to be between 150 and 665 N for posterior teeth (i.e. pre-molars and molars) [4] and 100 to 200 N for anterior teeth (i.e. canines and incisors). Generally, occlusal forces resulting from mastication are much lower than maximum biting forces. [29] In addition, the high posterior forces are not generally applied to the cusps of a single tooth. Forces are more likely distributed over the opposing cusps of several teeth. [4] Considering this, for a single posterior tooth, maximum loads of 70 to 150 N have been recorded during mastication and swallowing, but in generally these forces do not exceed 10 N. This would correspond to maximum load rates ranging from 700 to 1500 N/s and averaging 100 N/s. With loading cycles averaging 1 to 2 Hz, these values correspond to the tooth withstanding 6000 N/min. [29]

Assuming contact between opposing teeth (i.e. facets of similar material), simultaneous load application to four cusps resulting in circular contact areas with diameters ranging from 0.5mm to 3.00 mm, and a load range between 100 to 700 N, calculated contact stress (pressure) range from 3.5 to 890 MPa (0.0035 to .890 GPa). [4] The variation in stress resulting from masticatory loads as it relates to variations in enamel thickness due to the contours of the tooth [28] is also of clinical significance. For a clinical relevant investigation into the tooth response to mastication, an experimental design must incorporate variables of indenter size, load, and the influence of enamel thickness. An investigation of load rate may also be considered of clinical relevance.

2.2 Hertzian Contact

Hertzian Contact testing is a compression or indentation test. A normal compressive load is applied with a hard spherical indenter. It is classified as a blunt indentation method. It

simulates the key features of many practical contact events, such as occlusion. Damage initiation and evolution can be investigated on the microstructure scale of the tested material(s) using Hertzian Contact testing. [3] These characteristics of Hertzian Contact testing offer clinical relevance and provide insight into the relationship between damage mechanisms and material microstructure for dental applications [3, 4].

2.2.1 Theory

The theory of Hertzian Contact testing is rooted in a hard spherical indenter contacting a flat surface, applying a normal compressive load. Contact pressure increases monotonically with applied load. As load increases, the point of contact expands into a circle, creating a contact area. [3] At the onset of load application, the stress field is purely elastic [30, 31] and the indentation is referred to as "blunt"[32]. However, beyond a critical load the tested material becomes permanently damaged in the form of deformation and/or fracture [3].

Hertzian Contact specimens should be flat, with a polished surface. Observation of damage beneath the contact area may be achieved by one of two common methods. Specimens may be sectioned and polished into the contact area or the use of bonded interfaces [33] may be employed. Bonded interface specimens involve the bonding of the polished faces of two materials (materials bonded may be consist of multiple layers). In this case, contact is applied symmetrically across the interface of the two materials. This set-up is depicted in Figure 2.13. Post testing, the bond is broken (i.e. dissolved) and surface and sub-surface damage around and beneath the contact area is observed. This technique has some limitations in that the bond layer, although considerably thin (i.e. < 5

micrometers), prevents the full expansion/evolution of damage between the two halves of the specimens. [34]

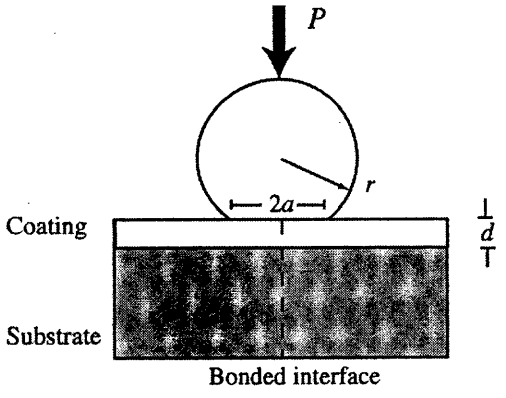

Figure 2.13 Diagram illustrating the bonded interface technique for Hertzian Contact testing. (Reproduced from Wuttiphan, S., *Contact Damage and Fracture of Ceramic Layer Structures*, in Department of Materials and Nuclear Engineering. 1997, University of Maryland. p. 157.)

In addition to the observance of the damage produced, Hertzian Contact allows for quantitative data collection and analysis. Independent variables are sphere radius (r) and indentation load (P). The dependent variable is contact radius (a), which can be measured from the residual imprint after indentation by coating the surface of the specimen with gold [35] or a film that will be removed upon contact with the indenter. These values allow for the calculation of the dependent variables of "indentation stress" and "indentation strain" [34]. Indentation stress is calculated as ($p_0=P/\pi a^2$) and indentation strain as (a/r).

2.2.2 Hertzian Characterization of Layer Structures

2.2.2.1 Monolithic Structures. In a very brittle (i.e. high elastic modulus) monolith material, if load is increased beyond a critical value, fractures are produced [3]. Fracture is, therefore, referred to as "brittle" mode damage [34]. At the onset of brittle mode

damage, fracture occurs on the surface of the test specimen. It initiates at a pre-existing surface flaw, which is subjected to tensile stresses, outside the contact area. The crack propagates along the surface around the contact area to form a surface "ring" crack. [3] Sub-surface, with increased load, the ring crack grows incrementally down the weakening tensile field, below the surface, and develops into a cone crack [36, 37]. If load is increased further and the border of the contact exceeds that of the surface ring crack, the sub-surface cone crack becomes engulfed in a compressive field and will close upon removal of the applied load [3].

In less brittle monolith materials, if load is increased beyond a critical value, deformation occurs. Deformation is "quasi-plastic" mode damage. At the onset of quasi-plastic deformation, damage occurs beneath the contact area due to sub-surface shear stress produced by the compressive loads. [3]

The quasi-plastic damage zones observed in heterogeneous microstructures are produced at weak boundaries with friction-resisted interfacial sliding by an array of discrete, closed "shear faults" [38, 39]. It occurs largely from fault sliding. This deformation is produced in several steps. [3] First, the development of cone cracks is suppressed by deflection of incipient surface ring cracks along the weakening tensile stress fields [37]. Next, local shear-induced sliding of micro-structural elements is induced at weak interfaces in the microstructure within the sub-surface compression field [38]. Microscopically, individual fault planes within the material microstructure are subject to net shear stresses, resulting from the difference between externally induced compression-shear fields and internal frictional resistance to sliding [40-42]. These fault planes may be the result of weak inter-grain or interface boundaries [43-46] or pre-

existing cracks or voids. Because sliding or slips of each fault is locally restricted or constrained by the surrounding elastic matrix, the shear displacements of individual fault planes are limited by the microstructure scaling of the faults.

The damage modes produced in monolithic structures are illustrated below in Figure 2.14.

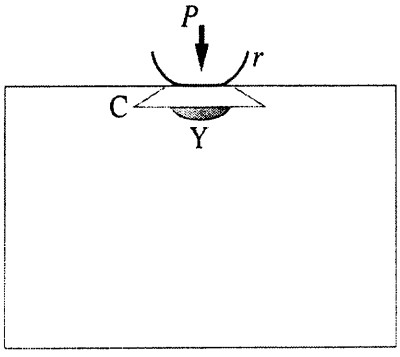

Figure 2.14 Diagram illustrating the damage modes and patterns observed in monolithic materials. (Reproduced from Lawn, B.R., *All-ceramic crown-like layer structures: characterization and design.* J Prosthet Dent, 2001.)

2.2.2.2 Bi-Layer Structures. In bi-layer structures, the damage modes and patterns produced are more complex [47, 48]. The material properties of each of the layers, the strength of the bond between the layers, and the geometry of the bi-layer structure greatly influence the type and extent of damage produced. The material property variable to be considered is the elastic-plastic (i.e. modulus) mismatch between the coating and substrate layer materials. The geometric variable to be considered is the thickness of the coating layer. [3]

If the coating layer is of significant thickness, the damage produced will be the result of the bulk properties of the coating layer and not the interaction of the bi-layer structure. Accordingly, a thick coating layer results in monolithic behavior. Damage is only observed in the coating thickness and only the microstructure of the coating layer

will determine the damage mode and patterns. If the coating layer is of lesser thickness, the damage produced will be the result of the interaction of the bi-layer structure. [3] In this case, the coating/substrate elastic modulus mismatch and the strength of the bond layer become key parameters to the damage produces and observed. Generally, Hertzian Contact testing is applied to bi-layer structures with significant coating/substrate elastic modulus mismatch.

In a bi-layer composed of a hard brittle coating layer (i.e. ceramic) supported by a soft less-brittle substrate (i.e. resin composite), both brittle and quasi-plastic damage modes may be produced [5]. In addition to the aforementioned brittle mode ring and cone cracks, a new, more dominant, fracture pattern is observed which is not seen in monolithic structures. At the undersurface of the coating layer, an array of radial cracks beneath the contact area, initiating at the interface and propagating towards the contact surface, are produced. Like other brittle mode damage, these radial cracks are the result of tensile stresses. Unlike the ring and cone cracks created as a result of tensile stresses resulting from compression at the surface, radial cracks are created as a result of tensile stress resulting from bending at the interface. Quasi-plastic mode deformation may be produced in both the coating and the substrate depending upon microstructure. [3]

If the bond between the coating and substrate of the bi-layer structure is weak, de-lamination of the coating layer from the substrate may occur at the interface. If the bond is strong, de-lamination does not occur. However, cracks propagating away from the surface (i.e. cone cracks) may penetrate into the substrate, where they will be arrested. [3] The damage modes generally produced in bi-layer structures relative to coating thickness are illustrated in Figure 2.15.

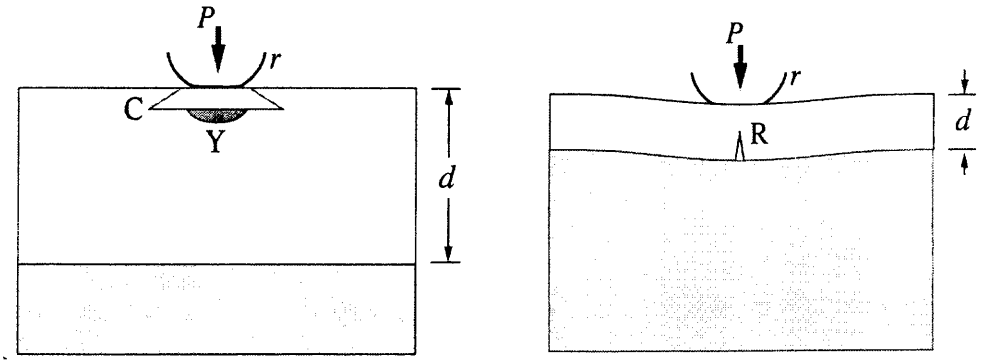

Figure 2.15 Damage modes generally produced in bi-layer structures relative to the thickness of the coating layer. (Reproduced from Lawn, B.R., *All-ceramic crown-like layer structures: characterization and design*. J Prosthet Dent, 2001.)

2.2.3 Hertzian Characterization of Dental Layer Structures

Hertzian contact has been used as a protocol for evaluation of the role of microstructure in the mechanical response of dental layer structures used for dental crown restorations [5]. It is more advantageous than traditional fracture testing methodologies for application to dental materials. Clinical variables of masticatory force and cuspal curvature identify closely with Hertzian variables of contact load and sphere (indenter) radius [1]. Accordingly, it more closely simulates the functional loading conditions [4] of dental restorations and teeth that most other fracture testing protocols, such as Vickers Indentation. Vickers Indentation is a sharp indentation that uses a diamond shaped indenter [3]; it does not correspond to the mechanics involved in the functional loading of teeth.

2.2.3.1 Monolithic Structures. Peterson, Pajares et al 1998 used bonded interface Hertzian contact testing to investigate the interrelationships between microstructure and the underlying mechanisms of failure relative to clinical function (i.e. occlusal loading) of ceramics proposed for dental restorations. The ceramics tested were representative of a

spectrum of dental ceramics having a range of well-characterized microstructures (i.e. homogeneous to heterogeneous). Employing the bonded-interface technique [33], using tungsten carbide spheres of radii ranging from 1.98 to 12.7 mm and single cycle loads of up to 5000 N, they found that these generic dental ceramics to exhibit two modes of contact damage: "brittle" mode and "quasi-plastic" mode. [34]

Brittle mode damage is characterized by fracture [34]. It is observed in the production of classic surface ring cracks and/or sub-surface cone cracks [34]. These fractures are a result of tensile stresses around the contact area created as a result of the compressive loads applied during testing [34]. Quasi-plastic mode damage is characterized by deformation. It is observed in the production of surface indentation (depression) below the contact area. This depression is the result of compressive-shear stresses. [3] The more homogeneous (less heterogeneous) the microstructure of a dental ceramic the more dominant mode of damage is brittle mode [3]. As micro-structural homogeneity decreases (i.e. heterogeneity increases), the more dominant mode of damage is quasi-plastic mode [3, 34]. [34]

2.2.3.2 Bi-Layer Structures. In bi-layer structures with coating/substrate mismatch, it has been observed [3, 47, 48] that coating fracture (i.e. brittle mode damage) is the dominant source of failure. Fracture is the result of tensile stresses concentrated on the surface near the contact area and sub-surface beneath the contact area. The extent of surface versus sub-surface damage observed is related to the extent of coating/substrate elastic-plastic mismatch and coating thickness. [5]

In bi-layers with considerable mismatch, the initial damage observed is sub-surface interface originated radial cracks. As load increases, both interface originated

radial cracks and surface originated cone cracks are observed sub-surface. This multiplicity of cracks is generally highly stable. [5]

Jung et al 1999 examined the hypothesis that contact load, coating thickness, and coating/substrate mismatch greatly influenced the damage produced and observed in clinically relevant dental layer structures subjected to Hertzian Contact testing. Hertzian contacts were used to investigate the evolution of damage in the coating layer as a function of contact load and coating thickness. Emphasis was placed on the sub-surface damage. [5]

In the bi-layer whose coating/substrate material properties best corresponded to enamel supported by dentin, sub-surface downward reaching surface initiated cone cracks were produced as well as upward extending interface initiated radial cracks. When the coating thickness was thick enough to cause the layer structure to act as a monolith, cone cracks were the dominant damage patterns observed. When the coating thickness was thin enough to cause the layer structure to act as a bi-layer, radial cracks were the dominant damage patterns observed. These cracks were highly stabilized and a wide range of loads necessary to cause initial cracking to total failure was observed. Clinically, this multiplicity of cracks stable cracks is comparable to tooth's ability to sustain hairline fractures in enamel without failure. [5]

2.2.4 Proposed Hertzian Characterization of the Tooth as a Bi-Layer

The dominant damage mode (i.e. brittle versus quasi-plastic) in any given material is dependent structure (i.e. monolithic vs. bi-layer) and upon the microstructure [3]. In bi-layer structures with considerable coating/substrate mismatch, it has been observed [3,

47, 48] that coating fracture (i.e. brittle mode damage) is the dominant source of failure. Brittle mode damage (i.e. tensile induced fracture) will tend to be produced in materials with fine microstructures and minimal internal weakness when subjected to Hertzian contact. Quasi-plastic mode damage (i.e. shear induced deformation) will tend to be produced in materials with coarse microstructures and greater internal weakness when subjected to Hertzian contact. [5]

In monolithic ceramic materials subjected to Hertzian Contact testing [32, 33, 35, 43, 44, 49], both brittle mode and quasi-plastic mode damage have been observed. The dominance of brittle mode damage versus quasi-plastic mode damage is dependent upon the microstructure of the tested material. In relatively hard, homogeneous microstructures, brittle mode damage dominates [3, 50]. Large sub-surface cone cracks are produced beneath the contact area [32, 49, 51]. In relatively tough, heterogeneous microstructures, quasi-plastic mode damage dominates [3, 50]. Deformation or damage zones are produced beneath the contact area [33, 35, 43, 45]. In structures of intermediate microstructures, both modes may be observed, with neither dominating [49, 51]. Brittle mode damage causes abrupt loss in strength. Quasi-plastic mode damage causes a more gradual loss in strength. Accordingly, heterogeneous materials are considered more damage tolerant. [50]

The human tooth is essentially a bi-layered structured. There is a high elastic-plastic mismatch between its bio-ceramic enamel coating layer and its bio-composite dentin substrate. Coating thickness of enamel varies across the surface of an individual tooth and from tooth-to-tooth. The microstructure of enamel is fine and is best described as heterogeneous. The bond between the two layers, the DEJ, provides a strong interface.

Therefore, it can be expected that both modes of damage to be present in comparable amounts in enamel supported by dentin, providing the bi-layer with appreciable damage tolerance.

Hertzian Contact theory and its application to monolithic and bi-layer structures composed of a material with coating/substrate mismatch and the effects of coating thickness for brittle ceramic materials with heterogeneous microstructures offers insight into what the expected response of the tooth may be to Hertzian contact. Initial Hertzian characterization of the human tooth as a damage tolerant bio-ceramic/bio-composite bi-layer structure is the aim of this thesis.

CHAPTER 3

MATERIALS AND METHODS

This chapter will present the study hypothesis and the study design to test the hypothesis. The experimental procedures will be outlined and discussed. The chapter will conclude with discussion of data collection and analysis techniques.

3.1. Study Hypothesis

Enamel supported by dentin will have the same response to Hertzian Contact testing as bi-layered structures of restorative dental ceramics and composites [5]. Independent variables of applied load and coating thickness will influence the dependent variables of contact radius, indentation stress, and indentation strain and determine the dominance and extent of damage modes and patterns observed.

Enamel supported by dentin will act as a monolithic ceramic layer when enamel thickness exceeds some threshold (i.e. >1.0 mm). When subjected to Hertzian Contact testing, the dominant mode of damage will be brittle mode. Surface ring cracks and sub-surface cone cracks will be observed. Sub-surface radial cracks will not be observed. Quasi-plastic deformation of enamel (i.e. coating layer) will also occur.

Enamel supported by dentin will act as a bi-layered structure composed of a hard brittle (i.e. ceramic) coating layer supported by a soft (i.e. composite) substrate when enamel thickness is below some threshold (i.e. <1.0 mm). When subjected to Hertzian Contact testing, the dominant mode of damage will be brittle mode. Sub-surface radial cracking will be the dominant brittle mode damage observed. Cracks will not penetrate

the DEJ. Some sub-surface cone cracks may be observed. Surface brittle mode damage may also occur. It may be observed as less pronounced or incomplete ring cracks. Quasi-plastic deformation will be observed in enamel (coating layer) only. De-lamination will not occur.

3.2 Study Design

Flat specimens of enamel supported by dentin were prepared from maxillary molar teeth. The enamel surface to be tested was polished to facilitate measurement of contact area and the visualization of damage. Hertzian Contact testing was performed on specimens and the surface and sub-surface (via sectioning) damage modes and patterns produced were observed for qualitative analysis. Measurements of the dependent variable of contact radius were made and used for the calculation of indentation stress and strain for of quantitative analysis.

The independent Hertzian variable of indenter size was held constant throughout all test trials. A tungsten carbide sphere of 1.58 mm radius was used as the indenter. This sized indenter is comparable to the smallest radius of the opposing cusps that make contact and apply force during functional loading [4]. It will produce the greatest damage, allowing for worse case investigation.

The independent Hertzian variable of load applied was varied throughout test trials. Trials were run with contact loads of approximately 50 N, 75 N, 100 N, and 150 N. These loads fall within the range of clinically observed maximum occlusal forces applied to posterior teeth [29].

The independent Hertzian variable, for bi-layer structures, of coating thickness was not controlled due to biologic variability. Enamel (coating) thickness was not known at the time of testing. Measurements were taken post-testing via sectioning.

Although not recognized as a Hertzian variable, the load rates used also varied throughout test trials. Trials were run with rates 18 N/min, 144 N/min, 288 N/min, and 576 N/min. These load rates fall below the observed clinical load rates, which are extremely high, averaging 600 N/min at the low end [4].

3.3 Experimental Procedures

3.3.1 Sampling of Teeth

The collection of samples (i.e. teeth) was achieved via convenience sampling. Extracted teeth were collected from dental clinics throughout the UMDNJ –Dental School at Newark. Maxillary molars free from restorations, caries, decay, or visible chipping and cracking were selected as samples. There was no information relative to the age, sex, or dental history of the persons from which the teeth were extracted.

3.3.2 Initial Processing of Teeth

Initial storage for collected samples was a solution of filtered and de-ionized water (fd H_2O) and < 1% bleach. From the supply of collected teeth, first and second maxillary molars free of restorations, caries, and decay were selected. For each specimen tested, a record was kept of the type of tooth. Selected specimens were placed in a 10% bleach solution for several hours to kill any bacteria or viral agents present. Once sterilized,

teeth were placed in a 1 molar phosphate buffer solution with calcium and magnesium (Quality Biological, Inc., Gathersburg, MD) and refrigerated. Teeth were used within three weeks of collection.

3.3.3 Specimen Preparation for Hertzian Contact Testing

After initial processing, specimen preparation began. Using a high-speed dental hand-piece with a diamond disk attachment, an initial flat was prepared on each tooth. The flat was prepared parallel to the long axis of the tooth to obtain a plane perpendicular to enamel rod orientation. The flat was prepared approximately 2 mm below the occlusal surface to obtain areas of enamel supported by dentin. The area or side of the tooth (i.e. buccal (towards the cheek), lingual (towards the tongue), mesial (towards the mid-line of the dental arch), or distal (away from the midline of the dental arch) upon which the flat was prepared varied from tooth to tooth. The decision as to which side of the tooth the flat was prepared on was dependent upon the ease of orientation of the diamond disk relative to tooth. For each specimen tested, a record was kept as to the placement of the prepared flat. Flat preparation averaged 30 seconds; moisture was maintained throughout the preparation.

Specimens to be tested via Hertzian Contact should be flat. The surface to be tested should be polished to facilitate measurement of contact area and the visualization of damage. In order to facilitate polishing, by providing a larger specimen size, the prepared teeth were embedded in a self-curing methyl methacrylate (Orthodontic Resin, Dentsply/Caulk Milford, DE). An ice-cube tray was used as a mold, allowing for the

embedment of several specimens at a time. Petroleum jelly was used to coat the interior of the mold to facilitate removal of the embedded specimens.

To maintain orientation relative to the prepared flat, dental wax was used to fix the flat to the base of the mold. Once fixed to the mold, the methyl methacrylate was mixed and poured over the teeth. Teeth were not covered entirely. To facilitate curing of the methyl methacrylate and to prevent drying of the teeth, the mold was placed into a 37° Celsius warm water bath. The portion of the tooth that was not covered by the methyl methacrylate insured maintenance of moisture of the embedded tooth. The mold remained in the water bath for approximately an hour to insure total curing. Each block containing an embedded tooth was numbered according to the record of its tooth type and the location of its prepared flat. Each block was removed from the mold. The dental wax was removed, exposing only the prepared flat on the face of the now poly methyl methacrylate (PMMA) block. Blocks were placed in fd H_2O.

Next, specimens were polished. Polishing was performed manually using the Ecomet 4 Variable Speed Grinder-Polisher (Buehler, Lake Bluff, IL). To obtain a larger area for testing, the face of each block was ground using a 600 Grit abrasive polishing sheet. Each block was ground using the 600 Grit paper at 40 RPM for an average of 2 minutes. Next, specimens were polished down consecutively with 6 micron, 3 micron, 1 micron, and ¼ micron diamond suspensions (Metadi ® Supreme Polycrystalline Diamond Suspension (Buehler, Lake Bluff, IL) at speeds of 40, 50, 60, and 70 RPM respectively for an average of 1½ minutes. Blocks were rinsed and placed in an ultrasonic bath (L & R Transistor/Ultrasonic T-14, L & R, Inc.) between each polishing step to remove particles that may have become trapped in the PMMA surrounding the

exposed enamel. Removal of particles/debris helped to better insure a nicely polished surface. Specimens were maintained moist throughout polishing.

The final step in specimen preparation was to section the embedded teeth to obtain flat and parallel specimens of enamel supported by dentin. Sectioning was achieved using the Isomet 1000 Precision Saw (Buehler, Lake Bluff, IL). Specimens were placed into mounts that allowed for orientation of the section and provided support throughout sectioning. The blocks were mounted with the polished face parallel to the saw blade. The saw used has an arm that allows for lateral movement of mounted specimens. The saw used allowed for setting of the speed of sectioning in RPM and the weight applied to the specimen during sectioning in pounds. Using the saw arm, blocks were moved laterally and positioned relative to the saw blade so as to insure the preparation of a flat and parallel specimen with a minimum total thickness of 3 mm. Blocks were sectioned at a speed of 400 RPM and with a weight of 125 grams. The saw is configured to lubricate as sectioning occurs, so the moisture of specimens was maintained. The sectioned face of each specimen (i.e. the side opposite the polished face) was ground using 600 Grit paper at 40 RPM for approximately 30 seconds to insure flatness of the specimen. After this final step in specimen preparation, specimens were once again placed in a 1 molar solution of phosphate buffer solution with calcium and magnesium. Testing of specimens occurred with several days of sectioning. A total of 40 specimens were prepared according to these methods.

3.3.4 Pre-Testing Processing of Specimens

Prior to testing, the flat and parallel polished specimens of enamel supported by dentin were imaged via the Olympus SZX12 (Olympus, Japan) stereoscope and Bioquant 98 (R & M Biometrics, Inc. – Bioquant, Nashville, TN), an imaging software, using trans-illumination for visualization and recording of pre-existing cracks. Once specimens were ready for testing, Accufilm IV (Parkell, Farmingdale, NY), a colored coating used for visualization of tooth-to-tooth contact in the mouth was placed on the polished enamel surface. This film is removed when indenter contact is made with the surface. It was employed to allow for visualization and subsequent measurement of the radius of the contact area resulting from Hertzian contact.

3.3.5 Hertzian Contact Testing of Specimens

Specimens were tested using the MTS 810 Material Test System (MTS Systems Corp., Minneapolis, MN). The MTS 810 is a hydraulic-powered testing device that allows for both tensile and compression tests with either load or displacement control. The load cell was placed in the upper grip and a testing stage was placed in the lower grip. A 1.58 mm radius tungsten-carbide ball (Small Parts INC., Miami Lakes, FL) was used as the hard spherical indenter for Hertzian Contact testing. The indenter was secured onto a metal rod (Benedikt Metal Products/Engineering/Tool Design, Rutherford, NJ), which was attached to the load cell. The testing stage (platform) was equipped with an x-y table (Benedikt Metal Products/Engineering/Tool Design, Rutherford, NJ), which facilitated positioning of specimens relative to the opposing indenter. The x-y table was equipped

with a right angle fence, which allowed for maintenance of orientation throughout positioning and testing.

The machine was operated under load control. In order to utilize load control, contact must be made with the test specimen prior to testing. The initial load at contact was difficult to control, but a reasonable range, relative to the loads applied, of 1 to 10 N was achieved. The system was programmed to apply a given compressive load at a given rate and to remove the load at a given rate to a prescribed level.

Successful testing was carried out on 37 of the 40 prepared samples. Specimens were considered successfully tested if the programmed load was applied at the programmed rate. An individual specimen was subjected to two Hertzian contacts if there was sufficient surface for a separation of at least 2 mm (i.e. > indenter radius).

Five specimens were tested at a load of 50 N and a rate of 18 N/min for a total of 8 Hertzian contacts. Five specimens were tested at a load of 75 N and a rate of 18 N/min for a total of 7 Hertzian contacts. Three specimens were tested at a load of 100 N and a rate of 18 N/min for a total of 4 Hertzian contacts. Four specimens were tested at a load of 150 N and a rate of 18N/min for a total of 4 Hertzian contacts.

Four specimens were tested at a load of 50 N and a rate of 144 N/min for a total of 5 Hertzian contacts. Four specimens were tested at a load of 75 N and a rate of 75 N/min for a total of 5 Hertzian contacts. Four specimens were tested at a load of 100 N and a rate of 144 N/min for a total of 6 Hertzian contacts. Four specimens were tested at a load of 150 N and a rate of 144 N/min for a total of 6 Hertzian contacts.

Two specimens were tested at a load of 100 N and a rate of 288 N/min for a total of 2 Hertzian contacts. Two specimens were tested at a load of 50 N and a rate of 576

N/min for a total of 2 Hertzian contacts. Two specimens were tested at a load of 100 N and a rate of 576 N/min for a total of 2 Hertzian contacts.

3.3.6 Light Microscopy: Initial Visualization of Contact Area

Post Hertzian testing, specimens were imaged via the Olympus SZX12 stereoscope and Bioquant 98 software package. If discernable, the contact area, as indicated by a circular absence of the applied colored film, was imaged at a range of magnifications. Using the superimposition of a calibrator slide at matching magnitudes, measurements of the contact diameter of the Hertzian contact were made. The contact radius (a) was determined from the measured contact diameter and recorded for quantitative data collection.

3.3.7 Post-Test Processing

After initial visualization of the contact area, the Accufilm was removed from the tooth surface via wiping and specimens were placed in fd H_2O. For further visualization of damage (i.e. cracks), a staining technique was employed. Silver nitrate is known to be an effective stain. Silver nitrate staining involves three steps: exposure to silver nitrate in solution, exposure to developer, and exposure to fixer. Silver nitrate in solution penetrates bulk structure and fills in voids (i.e. cracks). Developer chemically reacts with silver nitrate, which is clear in solution, and changes its color. Once developed, a specimen will appear dark in whatever areas or spaces the silver nitrate was able to fill. Prior to exposure to fixer, silver nitrate is light sensitive. Fixer, makes the staining more permanent. Once fixed, the silver nitrate is no longer light sensitive.

Within a dark box, specimens were stained, developed, and fixed. Specimens were stained with a 50% silver nitrate (Fisher Scientific, Fairlawn, NJ) solution for 20 minutes. The specimens were then rinsed and placed in a solution of developer for 10 minutes. Next, specimens were rinsed and placed in a solution of fixer for 20 minutes. Finally, specimens were removed from the dark box, rinsed, and placed in fd H_20.

Next, specimens were etched for approximately 10 seconds with 37% phosphoric acid etchant gel (3M Scothbond ™ – 3M Dental Products, St. Paul, MN). Etching removed the first few microns from the surface of the specimens. This resulted in the removal of a smear layer from the surface of the specimens. A smear layer is the thin buildup of material residue from polishing; it is generally a several microns thick. Removal of the smear layer removed surface residual silver nitrate and exposed the actual enamel surface, allowing for better visualization of surface damage and enamel microstructure.

In order to preserve the current state of the specimen for later reference, if necessary, a replica was made of the surface of the specimen. Making a replica was a two- step process. First, an impression/mold had to be made; this was achieved via the use of Impregnum F (ESPE America, Inc., Plymouth Meeting, PA), a dental polyether impression material. Impregnum F produces a mold with a precision on the order of one micron. The impression material was placed on the contacted surface and allowed to sit for approximately 45 minutes and then removed. Specimens were placed in fd H_20.

The next step in creating a replica would be the casting of the mold. The mold would be cast using a die epoxy. The epoxy would be poured into the mold as the mold rested on a vibrating table, which would serve to prevent the occurrence of air-bubbles in

the cast. The epoxy would be allowed to rest in the mold overnight to insure complete setting. Next, the cast would be removed from the mold, resulting in a near exact replica of the specimen.

3.3.8 Light Microscopy: Visualization of Surface Damage

Having been stained and etched, the specimens were imaged using the Olympus stereoscope for visualization of the surface damage at magnifications up to 108 times. Staining enhances the damage observed, and images were taken a multiple magnifications for qualitative data collection. Specimens were replaced in fd H_2O once imaged.

3.3.9 Specimen Preparation for Investigation of Sub-Surface Damage

In order to observe sub-surface damage, a cross-section at or through the contact area was prepared. Using the Isomet 4000 specimens were sectioned as they were in preparation of for testing. Specimens were mounted with the tested face perpendicular to the saw blade. The saw used has an arm that allows for lateral movement of mounted specimens. Specimens were positioned such that the cross-section produced was just outside the contact. Specimens were sectioned at a speed of 400 RPM and with a weight of 125 grams. The saw used lubricates as sectioning occurs, so the moisture of specimens was maintained. The portions of the specimens that did not contain the contact area were discarded. The portions of the specimens that contained the contact area were placed in fd H_20.

Next, the sectioned face of the specimens was polished. Specimens were manually polished using the Ecomet 4. To obtain a cross-section that was through or just outside of the contact area, the sectioned face of each specimen was ground using a 600 Grit abrasive polishing sheet. Each specimen was ground on 600 Grit paper at 50 RPM for an average of 2 minutes. Next, specimens were polished down consecutively with 6 micron, 3 micron, 1 micron, and ¼ micron diamond suspensions at 50, 60, 60, and 70 RPM respectively for an average of 1½ minutes. Specimens were rinsed and placed in an ultrasonic bath between each polishing step to remove particles that may have become trapped in the PMMA surrounding the exposed cross-section. Specimens were maintained moist throughout polishing.

3.3.10 Specimen Processing

For reasons previously stated in section 3.3.7, specimens were stained. Within a dark box, specimens were stained, developed, and fixed. Specimens were exposed to the 50% silver nitrate solution for 10 minutes. The specimens were then placed rinsed and placed in a solution of developer for 5 minutes. Next, specimens were rinsed and placed in a solution of fixer for 10 minutes. Finally, specimens were removed from the dark box, rinsed, and placed in fd H_20.

Next, the surface and cross-sectional face of the specimens were etched for approximately 5 seconds with 37% phosphoric acid etchant gel, allowing for better visualization of sub-surface damage beneath the contact area for reasons aforementioned in section 3.3.7. In order to preserve the current state of the specimen for later reference,

if necessary, a mold (impression), which included both surface and cross sectional faces, was made of each specimen.

3.3.11 Light Microscopy: Visualization of Surface and Sub-Surface Damage

Having been stained for enhancement of the damage produced, the specimens were imaged using the Olympus stereoscope for visualization of the surface and sub-surface damage. Images were taken of the surface and of the cross-sectional face. Cross-section images were used to measure the independent variable of enamel thickness in the method described in section 3.3.6 for the measurement of contact radius. In addition, angulated views of the specimens, which include both the surface and cross-sectional planes, were imaged. Images in all views and planes were taken at multiple magnifications (up to 108 times) for qualitative data collection. Specimens were placed in fd H_2O once imaged. If imaging illustrates that the cross-section prepared is not at or through the contact area, the specimen is subjected to the processing described in section 3.3.9 and this step is repeated.

3.3.12 Specimen Processing

In preparation scanning electron microscopy (SEM), the final step in the experimental procedure, specimens were mounted onto studs with colloidal graphite (LADD Research Industries, Burlington, VT). Once mounted, specimens were placed in a desiccator, which removes all moisture from specimens, overnight. Upon removal from the desiccator, specimens were carbon coated using a plasma coating system, the SEM Coating System

(Bio-Rad Polar Division, Cambridge, MA) with an E5000/E5100-374 Carbon Attachment (Bio-Rad Polar Division, Cambridge, MA).

3.3.13 SEM: Enhanced Visualization of Surface and Sub-Surface Damage

Specimens were imaged using the Hitachi S-2500 Scanning Electron Microscope (Hitachi, Tokyo) for higher magnification visualization of surface and sub-surface damage using the secondary electron imaging mode. The micro-structural elements of enamel, the DEJ, dentin, and damage patterns were more definitively discerned. Images were taken of the surface and of the cross-sectional face. In addition, angulated views of the specimens, which include both the surface and cross-sectional planes, were imaged. Images in all views and planes were taken at multiple magnifications, which were considerably higher than those obtained using the Olympus stereoscope, for qualitative data collection. Back-scatter imaging was used to verify silver nitrate presence in the cracks as a check for dessication induced enamel cracking in the vicinity of the indent. This was not found to be a problem. SEM imaging was the final step in the experimental procedure.

3.4 Data Collection

3.4.1 Qualitative Data

Light and scanning electron microscopy allowed for the visual investigation of damage. This allowed for investigation of the relationship between microstructure and mechanical response of the tooth to Hertzian contact. Comparisons were able to drawn between the

tooth's response and the response of clinically relevant dental layer structures. The study hypothesis was tested.

3.4.2 Quantitative Data

From the contact radius, a quantitative analysis of the damage induced via Hertzian contact testing was made. Values of indentation stress ($p_0 = P/\pi a^2$) and indentation strain (a/r) were calculated. Where (P) is the load applied, (a) is the contact radius, and (r) is the radius of the indenter.

3.4.3 Statistical Data

Teeth have high biological variability. Due to this high variability and the small sample sizes, relative to groups of specimens test at varying applied loads, load rates, and enamel thickness, statistical analysis methods were not applied. When appropriate, mean and standard deviations for the dependent variable were calculated.

3.5 Data Analysis

No significant measurements of the strength of the relationship between the independent variables of applied load, load rate, and enamel thickness and the dependent variables of contact radius, indentation stress, and indentation strain were made via statistical analysis. In analysis of qualitative data, both light and scanning electron microscopy were used to investigate the microscopic nature of the macroscopic damage produced. Microsoft Excel 2000 was used in analysis of quantitative data for the illustration of trends observed within the data.

CHAPTER 4

RESULTS

Thirty-seven specimens were tested successfully (i.e. the desired load was applied at the desired rate) tested. However, only 15 specimens (i.e. 18 contacts) were accepted as candidates for analysis. Specimens (contacts) were not included in analysis for several reasons. Hertzian contacts that were not confined to the polished enamel surface were rejected. This occurrence was the result of the inability to confine the Accufilm coating, applied prior to testing for post-test visualization of the contact area, to only the polished enamel surface. The rationale being, contacts not confined to the polished enamel surface would not properly test the response of the enamel/dentin bi-layer structure.

Specimens on which the contact area was not discernable, with the use of Accufilm and silver nitrate staining, were rejected. The rationale being, if the contact area was not known investigation of neither surface nor sub-surface damage around and beneath the contact area could not made. In addition, without measurement of contact radius, quantitative analysis could not be made.

Specimens on which the contact area was removed during sectioning or polishing were rejected. The rationale being, without investigation of the damage produced around and beneath the contact area relationships could not be drawn between qualitative and quantitative findings. Also, due to high biologic variability among specimens, any group (i.e. applied load and load rate) that contained only one contact was not considered for analysis

The 15 specimens (i.e. 18 contacts) available for analysis were not from each trial and were not in an equal distribution. Four specimens loaded with approximately 50 N at a rate of 18 N/min, resulting in 4 contacts for analysis. Four specimens loaded with approximately 75 N at a rate of 18 N/min, resulting in 4 contacts for analysis. Four specimens loaded with approximately 100 N at a rate of 144 N/min, resulting in 6 contacts for analysis. Three specimens loaded with approximately 150 N at a rate of 144 N/min, resulting in 4 contacts for analysis. It should be noted that multiple indents (i.e. contacts) on a given specimen are considered independent in analysis. Data for these 18 contacts can be found in Table A.1. This made determination of the effect of thickness, applied load, and load rate on the damage produced difficult. For this reason, this thesis is considered only an initial Hertzian characterization.

4.1 Qualitative Results

Surface and sub-surface examination of damage was performed. Damage was most pronounced in specimens tested at 18 N/min (i.e. low load rate). In fact, as the load rate increased, despite increases in load, the damage observed decreased. Both brittle mode and quasi-plastic mode damage were produced in specimens tested at the low load rate. Only brittle mode damage was observed in specimens tested at a higher load rate (i.e. 144 N/min). At the high load rate, brittle mode damage was minimal when compared to that produced at the low load rate. The presence and effects of quasi-plastic deformation, which appeared to play a role in the creation and propagation of complex fractures patterns, was notably observed in specimens tested at 18 N/min.

The surface of all specimens exhibited brittle mode damage. On the surface of most specimens tested, brittle mode damage was observed in the classic pattern of ring cracks. However, a non-classic multiplicity and expansion of concentric ring cracks was observed. This was most pronounced in those specimens tested at the low load rate. Figure 4.1 depicts this multiplicity and expansion in a representative specimen from the low load rate. Specimens tested at the higher load rates, exhibited considerably less multiplicity and expansion beyond the contact area. Figure 4.2 depicts this diminished multiplicity and expansion in a representative specimen from the high load rate.

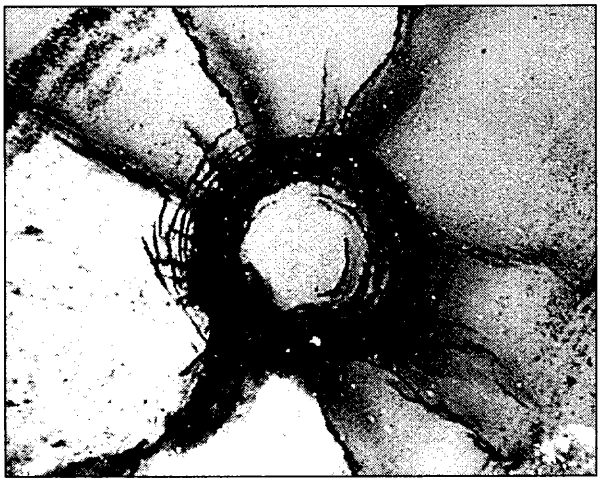

Figure 4.1 Light microscopy image of the enamel surface of a specimen tested to a load of 75 N at a load rate of 18 N/min. Magnification of 38.4x; contact radius of 0.425 mm.

Figure 4.2 Light microscopy image of the enamel surface of a specimen tested to a load of 150 N at a load rate of 144 N/min. Magnification of 60x; contact radius of 0.25 mm.

In addition to the ring cracks, a new pattern of brittle damage was observed on the surface of most specimens. Starburst like cracks, which radiate from the concentric ring cracks, were observed on the surface of most specimens. The distribution and the expansion of these cracks were greater in those specimens tested at the low load rate (refer to figure 4.1) as compared to the observed at the higher load rates (refer to Figure 4.2).

The sub-surface of the majority of specimens exhibited brittle mode damage. Downward reaching, surface originated cracks (i.e. cone cracks) were observed in most specimens. For specimens tested at the higher load rate (i.e. 144 N/min), these cracks were beneath and within the contact area. This is shown in Figure 4.3 in a representative specimen tested at the higher load rate. They did not propagate far below the surface (refer to Figure 4.3). For specimens tested at the lower load rate (i.e. 18 N/min), these cracks were generally difficult to discern do to complex pattern created from the sliding mechanism of quasi-plastic deformation. This is shown in Figure 4.4 in a representative specimen tested at the low load rate.

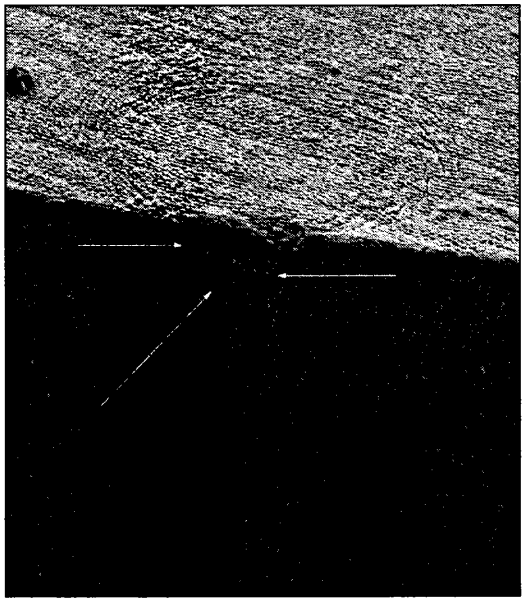

Figure 4.3 SEM image of the enamel in an angulated cross – sectional view of a specimen tested to a load of 100 Nat a load rate of 144 N/min. Magnification of 250x; contact radius of 0.125 mm.

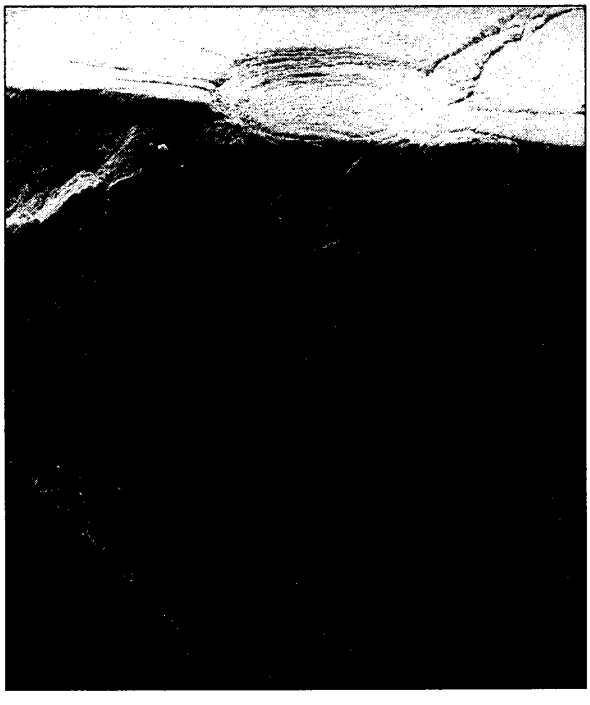

Figure 4.4 SEM image of the enamel in an angulated cross – sectional view of a specimen tested to a load of 75 N at a load rate of 18 N/min. Magnification of 20x, contact radius of 0.375 mm, enamel thickness of 1.3mm.

Upward reaching, interface originated cracks (i.e. radial cracks) were observed in most specimens. For specimens tested at the higher load rate, these cracks were less prevalent and less extensive than observed at the lower load rate. Radial cracks reaching the enamel surface appear to be the cause of the starburst pattern observed on the surface. This is shown below in Figure 4.5 in a representative specimen tested at the low load rate.

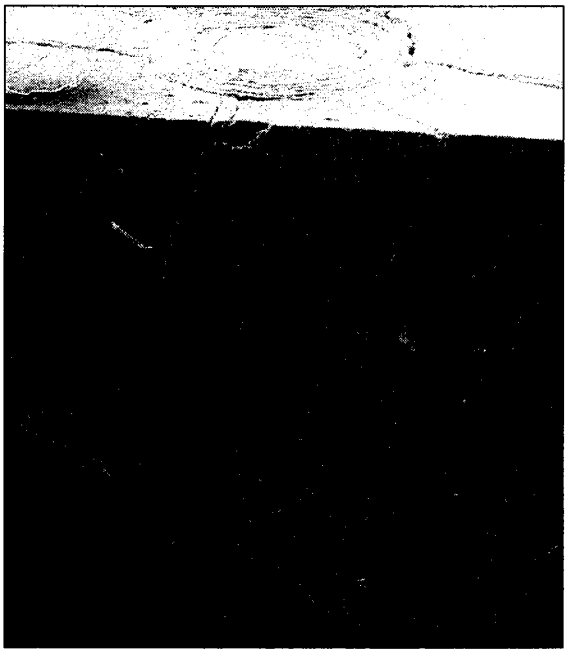

Figure 4.5 SEM image of the enamel in an angulated cross – sectional view of a specimen tested to a load of 75 N at a load rate of 18 N/min. Magnification of 80x, contact radius of 0.425 mm, enamel thickness of 0.95 mm.

Quasi-plastic mode damage was observed primarily in those specimens tested at the low load rate. Specimens tested at the high load rate exhibited elastic behavior. In those specimens tested at the low load rate, quasi-plastic deformation was observed in varying degrees and was observed as deformation in the form of a permanent indent or depression in the contact area. There appeared to be interrelationships of the concentric ring cracks and their sub-surface extension (i.e. cone cracks) with the observed

deformation, resulting in complex surface and sub-surface fracture patterns. This is shown in Figure 4.6 in a representative specimen tested at the low load rate. In those specimens tested at the higher load rate, the absence of quasi-plastic deformation appears to have resulted in less complex fracture patterns (refer to Figure 4.3).

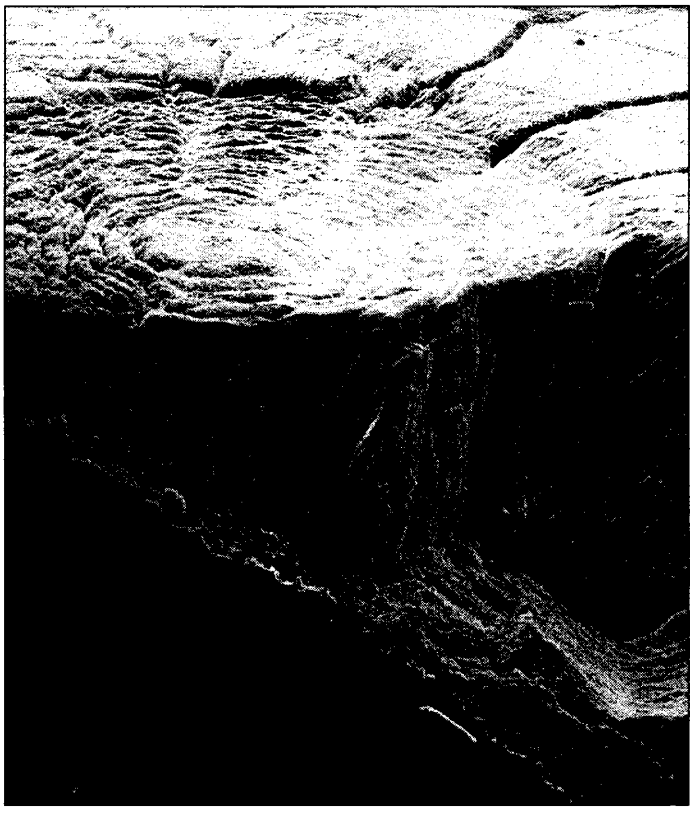

Figure 4.6 SEM image of the enamel in an angulated cross – sectional view of a specimen tested to a load of 75 N at a load rate of 18 N/min. Magnification of 120x, contact radius of 0.5 mm, enamel thickness of 0.4 mm.

4.2 Quantitative Results

Values of applied load (P), radius of indenter (r), and contact radius (a) were used to calculate values of indentation stress ($p_0=P/\pi a^2$) and indentation strain (a/r) for each specimen (contact). The relative elastic modulus for each specimen was calculated using the ratio of indentation stress to indentation strain. Specimens were grouped according

to the independent variables of applied load and load rate. Groups were arranged in this manner to facilitate investigation of the influence of load applied and the rate of application on the dependent variables of contact radius, stress, and strain. Within a given group, specimens were sorted according to the independent variable of enamel thickness. Sorting in this manner facilitated investigation of the influence of enamel thickness on the dependent variables of contact radius, stress, and strain. A full table of the groups can be found in Table A.1.

4.2.1 Among Groups

For each group, mean and standard deviations were calculated for enamel thickness, contact radius, indentation stress, indentation strain, and relative elastic modulus. Mean values among groups considered are presented below in Table 4.1.

Table 4.1 Mean values of independent and dependent variables among groups.

Applied Load (N)	Load Rate (N/min)	Number of Contacts	Enamel Thickness (mm)	Contact Radius (mm)	Indentation Stress (MPa)	Indentation Strain	Relative Elastic Modulus (MPa)
50	18	4	0.64 ± .34	0.49± .03	68 ± 9.05	0.31 ± .02	221 ± 46.3
75	18	4	0.78 ± .43	0.45 ± .06	123 ± 35.4	0.28 ± .04	455 ± 196
100	144	6	0.83 ± .36	0.23 ± .06	769 ± 641	0.15 ± .04	7059 ± 9389
150	144	4	0.65 ± .51	0.28 ± .02	2071 ± 2845	0.17 ± .01	11951 ± 16334

The first of the dependent variable investigated was contact radius, since it influences each of the other dependent variables. Inspection of the data, revealed no appreciable difference in contact radius for varying loads at the same rate. Averaging and comparing the dependent variable of contact radius between groups, independent of load, a general trend of decreased radius with increased rate was observed. Average

contact radius decreased by approximately one half with an 8 times increase in loading rate, resulting in a relatively shallow negative slope. This is illustrated in Figure 4.7.

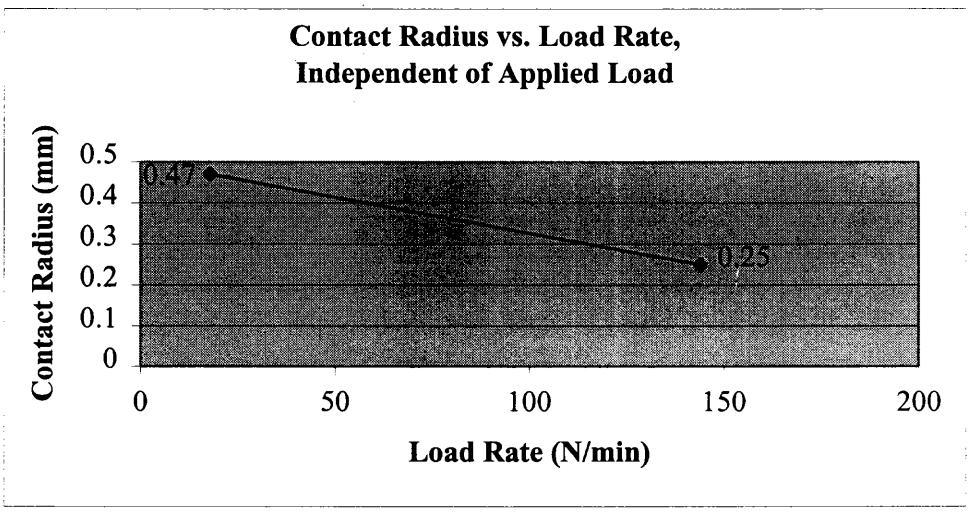

Figure 4.7 Plot of Contact Radius vs. Load Rate, Independent of Applied Load among groups.

The next dependent variable investigated was indentation stress. Inspection of the data, revealed appreciable differences in indentation stress for varying loads at the same rate. This is expected as a result of the direct relation between applied load and indentation stress. Comparing the dependent variable of indentation stress to applied load for a given rate, a general trend of increased stress with increased load was observed. Indentation stress for specimens tested at rate of 18 N/min increased by approximately 80 percent with a 50 percent increase in applied load, resulting in a positive slope. Indentation stress for specimens tested at a rate of 144 N/min increased by approximately 160 percent with a 50 percent increase in applied load, resulting in a more positive slope. These are illustrated in Figure 4.8.

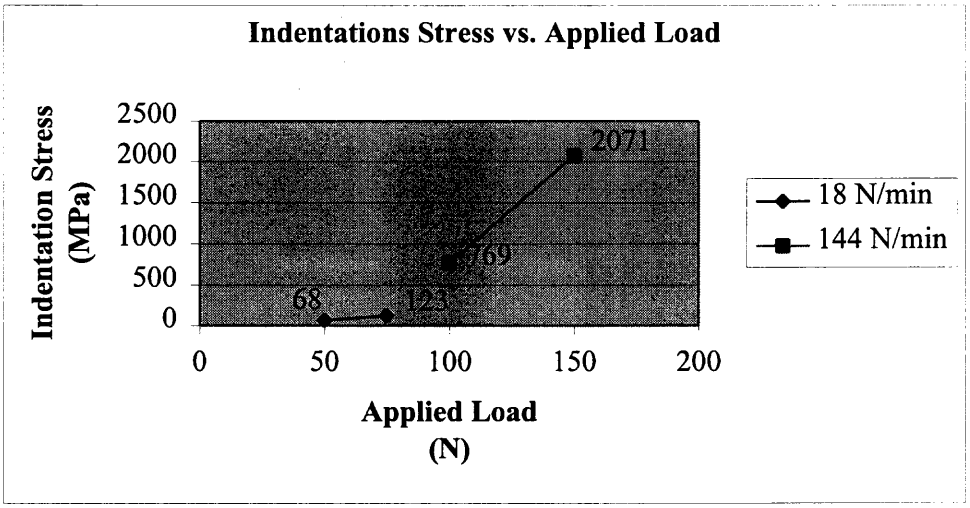

Figure 4.8 Plot of Indentation Stress vs. Applied Load among groups.

Further inspection of the data revealed a more appreciable difference in indentation stress for varying rates, independent of load. Averaging and comparing the dependent variable of indentation stress between groups, independent of load, a general trend of increased stress with increased load rate was observed. Indentation stress increased nearly 20 times with an 8 times increase in load rate. This is illustrated below in Figure 4.9.

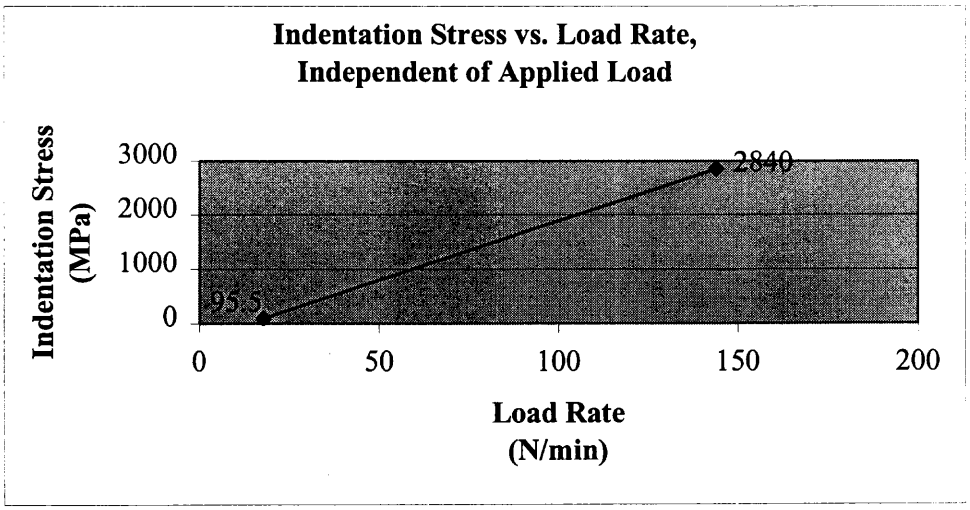

Figure 4.9 Plot of Indentation Stress vs. Load Rate, Independent of Applied Load among groups.

Indentation strain was the next dependent variable investigated. Given its direct relationship to contact radius, it was expected to observe a general trend of decreased strain with increased load rate, independent of load. This was confirmed upon inspection of the data, which showed no appreciable difference between strains for varying loads at a given rate. Indentation strain decreased approximately one half with an 8 times increase in load rate. This is illustrated below in Figure 4.10.

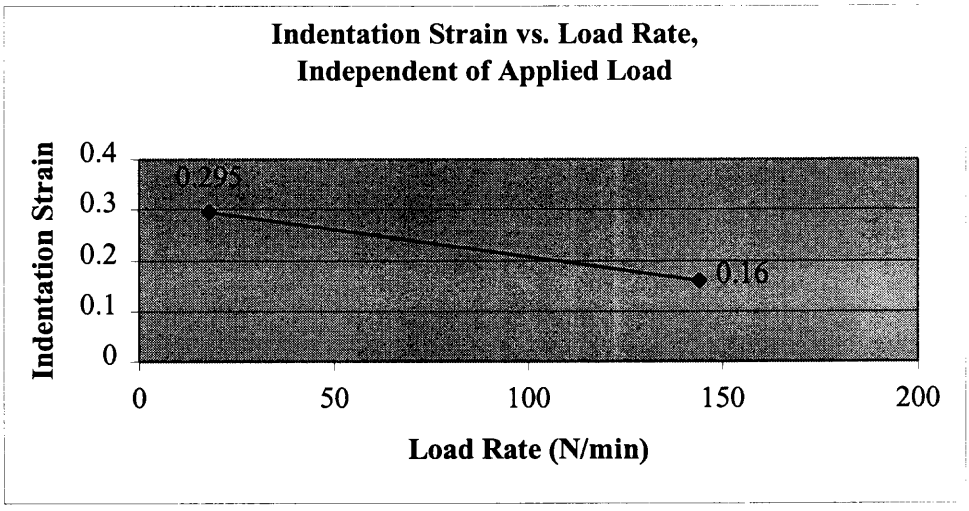

Figure 4.10 Plot of Indentation Strain vs. Load Rate, Independent of Applied Load among groups.

Relative elastic modulus, a ratio of the dependent indentation stress variable to the dependent indentation strain variable, was also investigated. Given the observance of opposite trends of stress increase and strain decrease for increases in load rate, the trend expected to be observed was not initially clear. Upon investigation of the data and an appreciation of the greater differences seen in indentation stress, it was expected to see a trends similar to those observed in indentation stress. The plots of relative elastic modulus vs. applied load and of relative elastic modulus vs. load rate, independent of

load are nearly exact to those for indentation stress (refer to Figures 4.8 and 4.9). These plots are illustrated in Figures A.1 and A.2.

Among groups, for the range of loads used and the rates at which they were applied, the independent variable of load rate appears to have a greater effect on the dependent variables of contact radius, indentation stress, and indentation strain. The dependence of these variables on load rate has not been found in the literature for Hertzian Contact response of layer structures. This finding may serve to broaden the scope of Hertzian characterization.

4.2.2 Within Groups

The contacts within a given group (i.e. applied load and load rate) were sorted according to enamel thickness. Within any given group, enamel thickness ranged from less than 1.0 mm to greater than 1.0 mm. Attention will be paid to detect any sensitivity to ranges of enamel thickness. The sorted list for each group is available in Table A.1. Given the quantitative results from among groups, and upon inspection of the data for within groups, no appreciable difference was found with varying loads for those specimens tested at 18 N/min. Accordingly, only data for specimens tested to an applied load of 50 N at a load rate of 18N/min was used to investigate the relationship between the independent enamel thickness variable and the dependent variables of contact radius, indentation stress, and indentation strain, as well as relative elastic modulus for specimens tested at the low load rate. The data for these specimens is found in Table 4.2.

Upon inspection of the data for within groups, an appreciable difference was found with varying loads for those specimens tested at 144 N/min. Accordingly, data for

specimens tested to applied loads of 100 N and 150 N at a load rate of 144 N/min was used for investigation of the relationship between the independent enamel thickness variable and the dependent variables of contact radius, indentation stress, and indentation strain, as well as relative elastic modulus for specimens tested at the high load rate. The data for these specimens is found in Tables 4.3 and 4.4, respectively.

Table 4.2 Data set for specimens tested to a load of 50 N at a load rate of 18 N/min.

Applied Load (N)	Load Rate (N/min)	Enamel Thickness (mm)	Contact Radius (mm)	Indentation Stress (MPa)	Indentation Strain	Relative Elastic Modulus (MPa)
50	18	0.25	0.525	58	0.33	176
50	18	0.5	0.5	64	0.32	200
50	18	0.75	0.475	71	0.3	237
50	18	1.05	0.45	79	0.28	282

Table 4.3 Data set for specimens tested to a load of 100 N at a load rate of 144 N/min.

Applied Load (N)	Load Rate (N/min)	Enamel Thickness (mm)	Contact Radius (mm)	Indentation Stress (MPa)	Indentation Strain	Relative Elastic Modulus (MPa)
100	144	0.3	0.25	518	0.158	3278
100	144	0.5	0.225	636	0.142	4479
100	144	0.9	0.3	359	0.19	1889
100	144	0.95	0.25	518	0.158	3278
100	144	1.1	0.25	518	0.158	3278
100	144	1.25	0.125	2066	0.079	26152*

*This specimen appears to be an outlier relative to the others, but is was included due to the known biological variability of teeth.

Table 4.3 Data set for specimens tested to a load of 150 N at a rate of 144 N/min.

Applied Load (N)	Load Rate (N/min)	Enamel Thickness (mm)	Contact Radius (mm)	Indentation Stress (MPa)	Indentation Strain	Relative Elastic Modulus (MPa)
150	144	0.3	0.25	774	0.158	4899
150	144	0.35	0.275	638	0.174	3667
150	144	0.55	0.275	638	0.174	3667
150	144	1.4	0.3	536	0.19	2821

The first group investigated was of those specimens tested with a load rate of 18 N/min to an applied load of 50 N (refer to Table 4.2). The first dependent variable investigated within this group was contact radius. Upon inspection of the data, a general trend of decreasing contact radius with increased enamel thickness was observed. This trend is illustrated below in Figure 4.11.

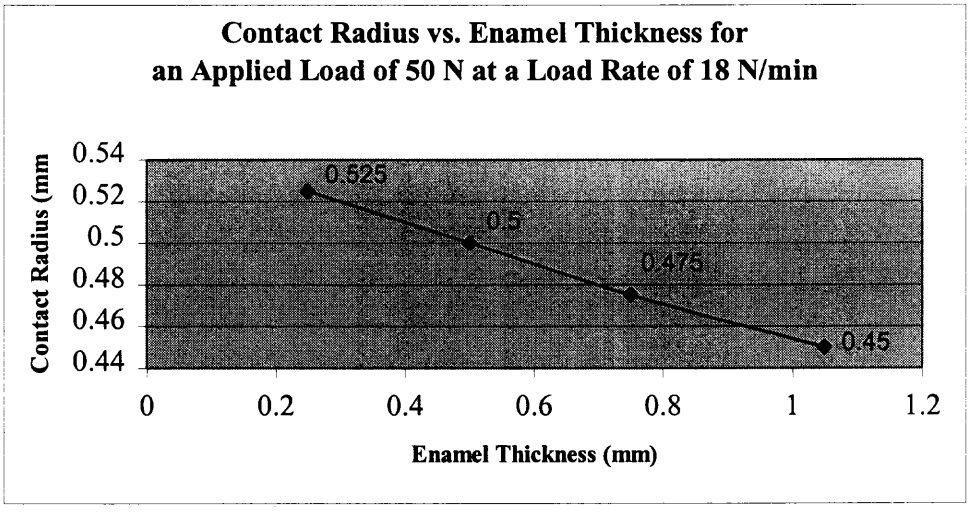

Figure 4.11 Plot of Contact Radius vs. Enamel Thickness for an Applied Load of 50 N at a Load Rate of 18 N/min.

The relationship between enamel thickness and indentation stress was investigated next. Upon inspection of the data, a general trend of increasing stress with increased enamel thickness was observed. This trend is illustrated in Figure 4.12.

The next relationship investigated was that of enamel thickness and indentation strain. Upon inspection of the data, a general of decreasing strain with increased enamel thickness was observed. This trend is illustrated in Figure 4.13.

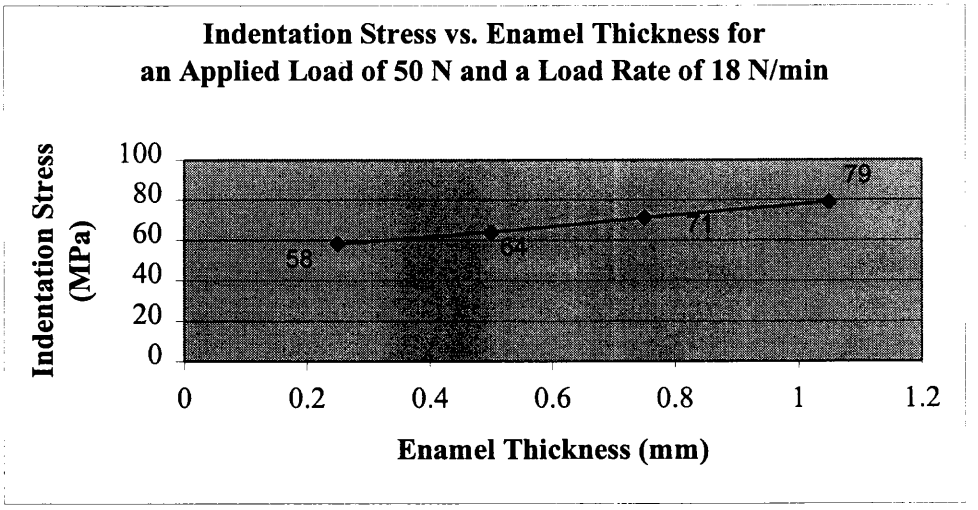

Figure 4.12 Plot of Indentation Stress vs. Enamel Thickness for an Applied Load of 50 N at a Load Rate of 18 N/min.

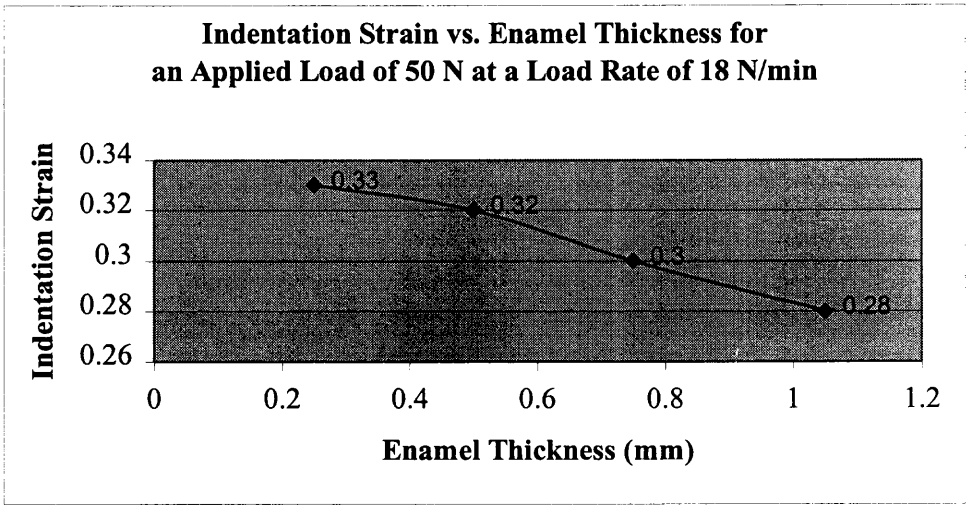

Figure 4.13 Plot of Indentation Strain vs. Enamel Thickness for an Applied Load of 50 N at a Load Rate of 18 N/min.

The relationship of relative elastic modulus to enamel thickness was also investigated. As in the cases among groups, this relationship shadowed that of indentation stress (refer to Figure 4.12). It is illustrated in Figure A.3.

Within the group of specimens tested at a load rate of 18 N/min to an applied load of 50 N, trends were not dependent on the range of enamel thickness. Increases or

decreases in dependent variables were consistent throughout the ranges of enamel thickness (i.e. < 1.0 mm and > 1.0 mm). The specimens tested at a load rate of 18 N/min to an applied load of 75 N (see Table A.2) demonstrated similar trends. These are illustrated in Figures A.4 – A.7.

The second group investigated was of those specimens tested with a load rate of 144 N/min to an applied load of 100 N (refer to Table 4.3). The first dependent variable investigated was contact radius. Upon inspection of the data, no general trend was observed. There was no evidence of relationship between the dependent variable of contact radius and the independent variable of enamel thickness. This is illustrated below in Figure 4.14.

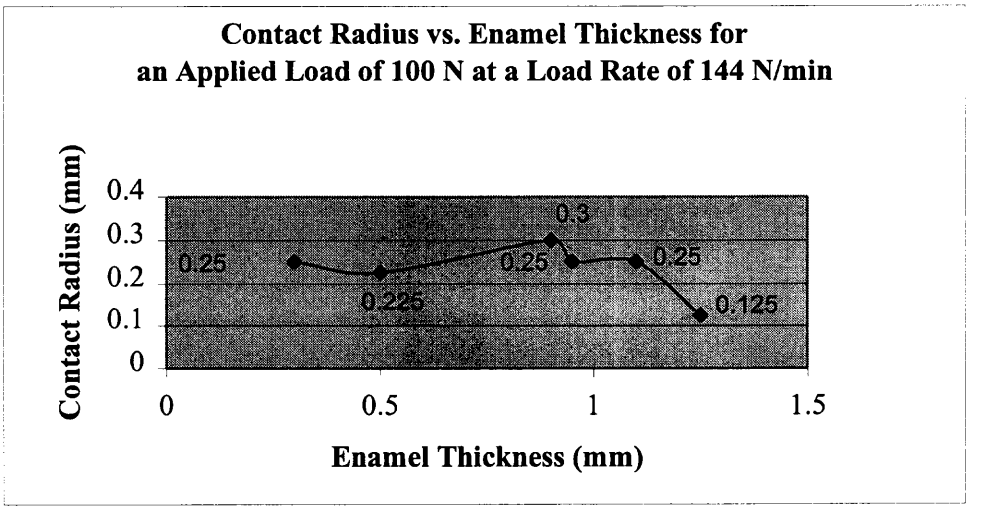

Figure 4.14 Plot of Contact Radius vs. Enamel Thickness for an Applied Load of 100 N at a Load Rate of 144 N/min.

Each of the other two dependent variables of indentation stress and indentation strain, as well as relative elastic modulus, was investigated relative to enamel thickness. Upon investigation of the data for stress, strain, and relative elastic modulus, no trends

were observed. There was no evidence of a relationship between indentation stress, indentation strain, or relative elastic modulus and enamel thickness. Illustrations of this were comparable to that shown for investigation of contact radius (refer to Figure 4.14); therefore they are not shown here. These illustrations may be seen in Figures A.8 – A.10.

The next group investigated was of those specimens tested with a load rate of 144 N/min to an applied load of 150 N (refer to Table 4.4). The first dependent variable investigated was contact radius. Upon inspection of the data, a general trend of increased contact radius with increases in enamel thickness was observed. This is illustrated below in Figure 4.15.

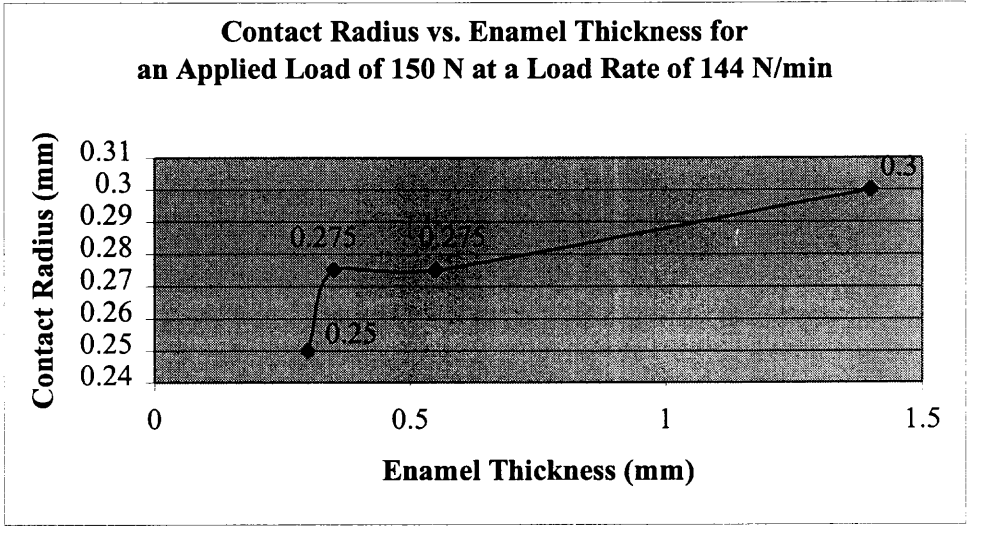

Figure 4.15 Plot of Contact Radius vs. Enamel Thickness for an Applied Load of 150 N at a Load Rate of 144 N/min.

The relationship between enamel thickness and indentation stress was investigated next. Upon inspection of the data, a general trend of decreased stress with increased enamel thickness was observed. This trend is illustrated in Figure 4.16.

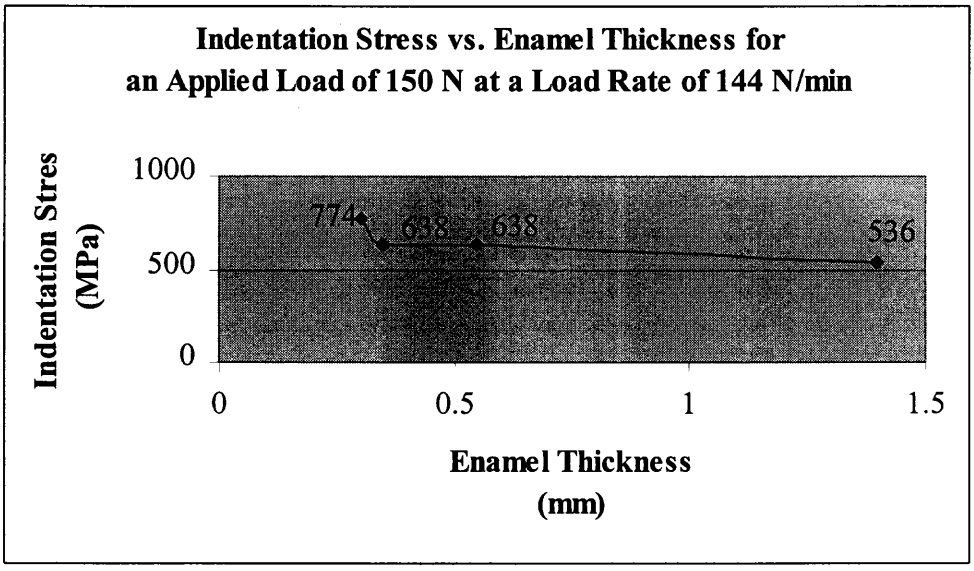

Figure 4.16 Plot of Indentation Stress vs. Enamel Thickness for an Applied Load of 150 N at a Load Rate of 144 N/min.

The next relationship investigated was that of enamel thickness and indentation strain. Upon inspection of the data, a general of increased strain with increased enamel thickness was observed. This trend is illustrated below in Figure 4.17.

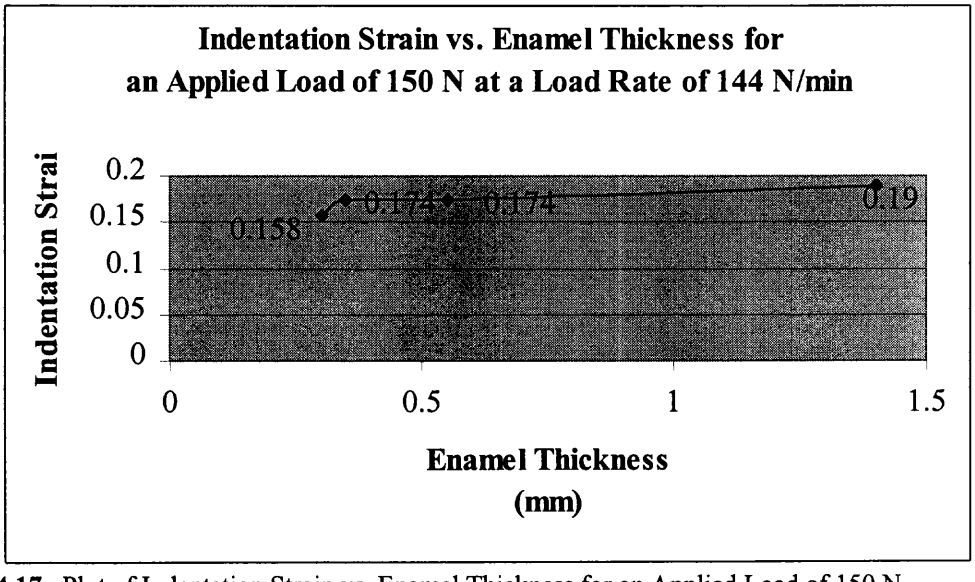

Figure 4.17 Plot of Indentation Strain vs. Enamel Thickness for an Applied Load of 150 N at a Load Rate of 144 N/min.

The relationship of relative elastic modulus to enamel thickness was also investigated. As in the cases among groups, this relationship shadowed that of indentation stress (refer to Figure 4.16). It is illustrated in Figure A.11.

Within the group of specimens tested at a load rate of 144 N/min to an applied load of 150 N, general trends for contact radius, indentation stress, indentation strain, and relative elastic modulus relative to enamel thickness were observed. There was no observed dependence upon ranges of enamel thickness. However, increases and decreases in dependent variables relative to the independent variable of enamel thickness were not as appreciable as the observed for those specimens tested at the low load rate. In addition, for this group, the trends observed were the opposite of those observed at the low load rate.

Within groups, the independent variable of enamel thickness appears to more appreciably affect/influence the dependent variables of contact radius, indentation stress, and indentation strain on those specimens in groups tested at the low load rate (i.e. 18 N/min). Enamel thickness appeared to exert some influence on dependent variables for those specimens tested to an applied load of 150 N at a load rate of 144 N/min. However, for these specimens the influence appeared to be to a much lesser extent and was also manifested in inverse relationships to those trends observed at the low load rate. Those specimens tested at a load rate of 144 N/min to an applied load of 100 N, no trends were observed relative to enamel thickness. None of these groups demonstrated any sensitivity to the ranges of enamel thickness. Possible reasons for this observance are offered in the proceeding chapter.

CHAPTER 5

DISCUSSION

It was hypothesized that enamel supported by dentin would have the same response to Hertzian Contact testing as dental layered structures, namely bi-layered structures of dental ceramics and resin composites used for restorations. Under, this hypothesis, independent variables of applied load and coating thickness, were expected to influence the dependent variables of contact radius, indentation stress, and indentation strain. The damage modes produced (i.e. brittle and quasi-plastic) and the extent to which they are observed were expected to be determined by whether or not the system (i.e. enamel supported by dentin) responded as a monolithic structure or as a bi-layer structure. The behavior of the system as a monolith or as a bi-layer was expected to be the result of coating (i.e. enamel) thickness. It was expected to observe a threshold value of enamel thickness, below which the system responded as a bi-layer (i.e. enamel supported by dentin) and above which the system responded as a monolith (i.e. enamel only). This hypothesis and its inherent expectations were not fully supported.

The main points of dispute were with respect to the dependence of the type and extent of damage modes produced and patterns observed. The observance of both brittle mode and quasi-plastic modes was in support of the hypothesis. However, the same dependence upon thickness and load for determination of the dominance between modes and within modes, specifically brittle mode, was not observed. What was observed was a strong dependence on load rate (i.e. low vs. high), a variable not previously investigated in dental applications of Hertzian Contact.

Enamel supported by dentin loaded subjected to applied loads of 50 N and 75 N at a load rate of 18 N/min (i.e. low load rate) had a different Hertzian response than enamel supported by dentin subjected to applied loads of 100 N and 150 N at a load rate of 144 N/min (i.e. high load rate) (see figures 4.1-4.6). Seemingly independent of load, specimens loaded at the low load rate displayed less damage tolerance (i.e. a greater accumulation of damage) than those loaded at the high load rate. These results revealed visco-elastic behavior of the tooth (i.e. enamel supported by dentin). At high load rates, elastic behavior dominated rather than brittle (i.e. fracture) and quasi-plastic (i.e. deformation). At low load rates, brittle and quasi-plastic behavior dominated.

At both load rates, enamel supported by dentin behaved as a bi-layer structure, relative to the damage modes and patterns predicted by Hertzian theory and its application to dental layer structures. No sensitivity to enamel thickness ranges (i.e. monolithic vs. bi-layer response) was observed. This can be the result of the range of enamel thickness of the specimens; the threshold for strictly monolithic behavior may not have been present.

At the low load rate, influences of enamel thickness were appreciably observed among variables of contact radius, indentation stress, and indentation strain, but the same influence was observed at the high load rate. At the low load rate, it is believed that enamel microstructure was less able to accommodate damage (i.e. damage modes and patterns). Therefore, thickness (i.e. bulk enamel) was able to influence behavior. Given the extent of damage produced in those specimens tested at the low load rate, they will primarily be used for discussion on the relationship between fracture and deformation patterns and enamel microstructure observed in response to Hertzian contact.

Comparisons will be made to patterns observed in dental ceramics and other brittle materials.

At the high load rate, the absence or small and negative influence of enamel thickness (i.e. bulk enamel) on the variables of contact radius, indentation stress, and indentation strain is believed to be due to the ability of enamel microstructure to exert its influence over the damage mechanisms (i.e. modes and patterns). At the high load rate, enamel behaved elastically, which resulted in less damage accumulation. This visco-elastic behavior offers inference into the influence of enamel architecture on the micrometer and nanometer scale; therefore enamel acting in bulk (i.e. thickness dependent) would diminish this elastic behavior and cause damage to accumulate at the high load rate. Discussion of the possible role of enamel microstructure and nano-structure on visco-elasticity, as observed at the high load rate, will be given.

Considerable effort has been put forth for the development of analytical expressions for the critical loads to initiate cone cracking and radial cracking under single-cycle loading Hertzian Contact in ceramic layer structures. [2] The critical load for initiation of cone cracks is predicted by [37, 50, 52]

$$P_C = A(T_c^2/E)r \tag{5.1}$$

where A is a dimensionless coefficient, T_c, which is commonly termed K_{Ic}, is the toughness of the ceramic, E is the elastic modulus, and r is the radius of the indenter [2]. Toughness is a dominant parameter because it is the toughness of the ceramic that largely determines the resistance to the sub-surface propagation of a surface ring into full cone crack initiation. [52] The radius of the indenter is a parameter in this case because the smaller the indenter the less blunt the indentation, the greater the damage produced.

Using A of 8.6 x 10^3 [2], T_c = 1.30 MPa.m ^{½} [16], E = 85 x 10^3 MPa [16], and r = 1.58 mm, P_C was determined to be approximately 270 N for enamel.

For a thin ceramic coating over a low modulus substrate, classic elasticity solutions for the stresses in a surface-loaded flexing plate on compliant foundation can be used as a basis for analysis of radial cracking. [2] Equating the maximum tensile stress at the lower surface of the flexing plate to the strength (i.e. tensile strength) σ_c of the ceramic coating produces a prediction for the critical load for the initiation of radial cracking as [52, 53]

$$P_R=B\sigma_c d^2/\log(E_c/E_s). \quad (5.2)$$

B is a dimensionless coefficient, d is the thickness of the ceramic coating, E_c is the elastic modulus of the coating, and E_s is the elastic modulus of the substrate. In theory, with increases in P (i.e. applied load) beyond P_R, radial cracks can expand stably until they penetrate the surface of the coating. [2] Using a B of 2.0 [2], σ_c = 20 MPa [16], d=1.0 mm, and E_c/E_s = 6 [16], P_R for enamel supported by dentin was determined to be approximately 50 N.

These relationships (5.1 and 5.2) have been shown to hold for dental ceramics (i.e. dental porcelain, glass infiltrated alumina, and zirconia) [2]. In the case of enamel supported by dentin, they do not predict the onset of cone cracking well, primarily at the low load rate. They do predict the onset of radial cracking relatively well, primarily at the low load rate. For specimens tested at 18 N/min, both cone and radial cracking were present at a load as low as 50 N. Given the extensive cone cracking observed, it is believed that at the low load rate, P_C is considerably lower than predicted by the equation (5.1). Given the observance of surface penetration of radial cracks, which is theorized to

occur once P exceeds P_R, at loads as low as 50 N for the low load rate, it is believed that at the low load rate P_R is relatively lower than predicted by the equation (5.2).

For specimens tested at 144 N/min, at loads of 100 N, radial cracking and cone cracking were present, but to a lesser degree than the observed at 150 N for the same rate and to a much lesser extent than the observed at the low load rate. Given the modest cone cracking observed, it is believed that at the high load rate, P_C is also lower than predicted by the equation (5.1). Given the diminished surface penetration of radial cracks, which is theorized to occur once P exceeds P_R, at loads as high as 150 N for the high load rate, it is believed that for the high load rate P_R is comparable to that predicted by the equation (5.2). Thus, in the case of enamel supported by dentin, it appears that load rate has the ability to alter the behavior of the ceramic coating and, thereby, alter the onset of cone and radial cracking; causing enamel supported by dentin to behave differently than comparable dental layer structures.

The brittle mode damage (i.e. fractures) produced in the enamel was not expressed in the precise same damage patterns (i.e. ring, cone, and radial cracks) as those produced in the brittle coatings of the dental ceramic layer structures. Damage patterns were comparable, but variations arose relative to the complex microstructure of enamel, namely the gnarling (i.e. undulating) of groups of enamel rods and the decussation (i.e. intertwining) of groups of enamel rods. These micro-structural elements influenced the patterns of macroscopic damage produced.

A multiplicity of concentric ring cracks are observed on the surface of all specimens tested at the low load rate. These cracks appear within the deformation zone (i.e. indentation) and extend beyond it. Within the indent, concentric ring cracks appear

as a circular set steps, with the highest level ending at the periphery of the deformation. (refer to Figure 4.6) This pattern of brittle mode fracture has not been observed in heterogeneous dental ceramic layer structures. In such heterogeneous ceramic layer structures, the deformation (quasi-plasticity) occurs without ring and subsequent cone cracking. However, it was observed in other layer structures of brittle materials on soft substrates [54]. However, this pattern was only observed with very high loads (4000 N) [54]. In enamel supported by dentin, this was observed at loads of 50 N and 75 N when at the low loading rate.

At high magnification, these ring cracks did not appear as perfect circles, which is the shape generally observed in homogeneous brittle ceramic dental layer structures. Instead, deviations from a totally circular path were observed relative to the course of groups of enamel rods. An example of this is seen in Figure 5.1. In cross-section, these concentric ring cracks appeared to be the result of or influenced by shear stress induced sliding/shifts (i.e. quasi-plastic deformation) in layers of enamel rods (refer to Figures 4.4 and 4.6). The resulting interaction of brittle mode and quasi-plastic mode damage, unobserved in the coatings of other brittle layer structures, appears to be the result of the inherent microstructure of enamel.

Figure 5.1 SEM image of the enamel surface of a specimen tested to a load of 50 N at a load rate of 18 N/min. Magnification of 100x; contact radius of 0.45 mm.

In cross section, radial cracks were observed to extend upward toward the enamel surface in varying degrees relative to their location to the contact area (i.e. indent). Directly beneath the contact area, which is seen on the surface as an indent (i.e. deformation zone), radial cracks did not generally extend the full thickness of the enamel. Their path, like the other cracks observed, deviated from the expected path, which in the case of radial cracks, a relatively straight vertical path from the interface towards the surface. In contrast, the radial cracks observed had a tortuous path upward into the enamel (refer to Figure 4.5). The gnarling of individual enamel rods had the most influence given the vertical nature of the crack. In the proximity of the DEJ, where these cracks initiate, gnarling of enamel is peaked. Given that radial cracks are a key player in total fracture of brittle coatings in dental and other layer structures, the microstructure of the tooth once again offers the structure some damage tolerance via built-in fracture resistance.

The gnarling of enamel rods does not appear as the only limiter of radial crack extension. Recognizing that a radial crack, although visualized in two dimensions in cross section, is three dimensional, it can be conceived that the sliding of layers of enamel rods, which occurs beneath the contact area (i.e. the indent) also limits the propagation of radial cracks. This is supported by the observance of radial cracking outside of the contact area, which is not beneath the deformation zone produced by shear induced sliding of layers of enamel rods. These radial cracks located laterally to the contact area (i.e. deformation zone) are observed to extend the full thickness of the enamel (refer to Figure 4.5).

On the surface, their three-dimensional nature is evident in the creation of a star-burst pattern, analogous to the spokes of a wheel, radiating generally from the ring cracks located at the periphery of the deformed (i.e. indented) contact area (refer to Figure 4.1). Producing a new pattern of surface cracking as they penetrate the surface, which is predicted when applied loads exceed the critical load (P_R) for radial crack initiation [2]. From the surface, the role of enamel decussation in the crack propagation of radial cracks is observed. The paths of these cracks do not follow a straight coarse. Assuming propagation along the path of group of enamel rods, decussation, which conceptually can be thought of as three–dimensional gnarling of groups of enamel rods, results in the production of an undulating cracks path relative to the paths of a given group of rods (refer to Figure 4.1). Although predicted by theory [2], the observance of surface eruption of radial cracking is not found in the literature. However, the basic mechanisms proposed for its production, namely full thickness eruption of radial cracks, are alluded to and supported by work done on bi-layers with large coating/substrate mismatch [53].

Chai et al 1999 examined a range of radial crack patterns over a various regions in a model brittle coating system with high coating/substrate modulus mismatch, using Hertzian Contact. The use of transparent coating and substrate materials allowed for in-situ visualization of crack initiation and evolution in the coating layer [53]. Variations in coating thickness, (d), was used to investigate the morphology of radial crack patterns; indenter size was a constant. Attention was paid to intermediate thickness ranges (i.e. 0.05 mm<d< 2 mm) corresponding to monolithic behavior versus bi-layer behavior of the system. Two brittle mode damage patterns were observed: sub-surface radial cracks and surface circumferential ring cracks. The radial cracks observed were initiated at the interface between the coating and substrate, along the contact axis (i.e. beneath the contact area), proximity to the contact axis was found to be dependent upon thickness. The ring cracks observed were initiated at the surface outside of the contact area, proximity to the contact area was found to be dependent upon thickness. [53]

When the system behaved as a monolith (i.e. at the upper end of the intermediate coating thickness range), surface ring cracks initiated just outside the contact area (i.e. conventional Hertzian response), but were able to expand beyond the contact area depending upon the presence of surface flaws. When the system behaved as a bi-layer (i.e. at the lower end of the coating thickness range), both surface ring cracks and median-radial cracks were highly localized about the contact [55]. Both crack types were highly-stable, making penetration through the coating into the substrate difficult [3].

Median-radial cracks appeared capable of being the dominant crack pattern over a range of coating thicknesses as predicted by the work of Chai et al 1999. Radial cracks were seen to extend laterally along the interface as well as longitudinally [3, 47, 48]

upward from the interface. However, the radial cracks observed remained entirely confined to the sub-surface of the coating layer throughout their evolution. It was found that these sub-surface median-radial cracks initiated prior to surface ring cracks. However, the prevalence of surface flaws may cause the reverse to occur. When ring cracks were initiated prior to radial cracks, their radii were seen to be on the order of one magnitude higher than that of the contact area in the reverse case. This work predicted that similar radial crack patterns would dominant and other bi-layer systems with brittle coatings on less brittle, more compliant substrates such as in teeth. [53]

These predictions were found to hold for enamel supported by dentin. Given that the ring cracks extended beyond the contact area and appeared un-interrupted by the erupted radial cracks as depicted in Figure 5.2, it is the contention that ring cracks were formed prior to the penetration of radial cracks to the surface. This may be the result of the presence of surface flaws, which were either pre-existing or creating during specimen preparation [53]. The observance of cracks extending the full thickness of the enamel may be due to the range of enamel thickness for the specimens tested or the extent of tensile stresses created at the interface or the result of loads increasing significantly beyond the critical load to radial cracking initiation. [2]

Figure 5.2 Light microscopy image of the enamel surface of a specimen tested to a load of 75 N at a load rate of 18 N/min. Magnification of 38.4x; contact radius of 0.5 mm.

The damage modes and patterns observed in specimens tested at the high load rate can be considered the same as those observed at the low load rate, but to a much lesser degree. Quasi-plastic deformation was virtually non-existent. Brittle mode damage (i.e. fracture) was observed. Surface ring cracks were present, but the multiplicity observed at the low load rate was not observed. Most were not observed to form complete rings. In addition, expansion beyond the contact area did not occur (refer to Figure 4.2). The decreased multiplicity and expansion of ring cracks is believed to be the result of the absence of the shear-induced sliding which results in quasi-plastic deformation. Thus, supporting the concept of an inter-relationship between the ring-cracks and deformation zones as discussed relative to the observed patterns at the low load rate.

Sub-surface, cone cracks were observed beneath the contact area (refer to Figure 4.3). As this was not observed at the low load rate, in the presence of quasi-plastic

deformation, it is believed that quasi-plastic deformation dominates brittle mode fracture when they co-exist in enamel. The paths of cones cracks were determined by the same micro-structural mechanisms as they were at the low load rate.

Radial cracking was present, but less extensively than was observed at the low rate. This is likely the result of the an inability of radial cracks to initiate or propagate due to rapid applications of load, that is the bending mechanics at work to create radial cracking were on a time scale not much greater than the time it took to apply the loads at the high load rate. As a result, the starburst pattern (i.e. the surface eruption of radial cracks) was observed to a much lesser degree. The distribution of these cracks was no longer analogous to spokes of a wheel in that they no longer spanned the entire circumference of the ring cracks. They were generally found to radiate strongly from within the innermost ring crack (refer to Figure 4.6). As this was not observed at the low load rate, where the presence of quasi-plastic deformation absorbed the energy necessary for extension of radial cracking beneath the contact area, the contention of quasi-plastic deformation dominance over brittle mode fracture. The paths of these radial cracks appear to be determined by the same micro-structural mechanisms as they were at the low load rate.

Observance of less accumulation of damage at the high load rate, as compared to at the low load rate, appears to be largely due to the absence of quasi-plastic mode damage (i.e. deformation). The virtual absence of deformation is the result of elastic behavior. Given the dependence upon load rate (i.e. time), the absence of deformation in enamel supported by dentin is the result of visco-elastic (i.e. time dependent elasticity) behavior (i.e. properties).

Visco-elasticity is a known property of proteins and other organic materials such as collagen. Within enamel, organic material is found in only small percentages. In enamel, which is predominantly an inorganic material, organic material is found on the micro-structural and nanometer scale surrounding rods/interrods and enveloping individual hydroxyapatite crystallites respectively. The concentration being within the tail area of enamel rods and the interred (rod sheath), which is protein rich [56, 57]. These areas believed to be weak interfaces, due to discontinuity of crystalline orientation and the presence of soft organic matter. Accordingly, cracks generally propagate relative to these as they present a path of least resistance (refer to Figure 2.9). In addition, the collagen fibrils that are within the DEJ may have some influence on the observed visco-elastic behavior. At low load rates, their visco-elastic behavior would serve to produce quasi-plastic deformation, whose mode of operation is shear-induced sliding between layers of enamel rods relative to these structures. [58] The visco-elastic properties of dentin are well known [59], but there has been no presentation in the literature regarding visco-elastic behavior of enamel. This remains to be investigated in further detail via such methods as Hertzian Contact testing.

CHAPTER 6

CONCLUSIONS AND FUTURE WORK

The tooth's response to Hertzian Contact Testing is complex. Classic Hertzian brittle and quasi-plastic damage modes are produced in structures of enamel supported on dentin. These damage modes are observed in fracture and deformation patterns that correspond to characteristic patterns observed in dental ceramics and layer structures that have been characterized by Hertzian Contact. However, distinctions and new findings, arise as dependence upon the unique microstructure of enamel is considered. While the same mechanisms of fracture (i.e. tensile stresses) and deformation (i.e. shear stresses) were evident in the production of brittle mode and quasi-plastic mode damage respectively, accommodation of enamel microstructure and its micro-structural sensitive properties resulted in deviations from the hypothesized Hertzian response.

The dominance of fracture (i.e. brittle mode damage) and deformation (i.e. quasi-plastic mode damage) were found to be more dependent upon the rate of load application than the traditional Hertzian independent variable of applied load. With increased load rates, elastic behavior rather than brittle or quasi-plastic behavior was observed in and dominated the tooth's (i.e. enamel supported by dentin) response to Hertzian contact. The introduction of the new variable of load rate, expanded the scope of Hertzian characterization of enamel supported by dentin, allowing for the elucidation of elastic properties and mechanisms of operation. Traditional Hertzian variables of applied load and coating thickness, which are predictors of damage for brittle and quasi–plastic modes, were found to have little influence on the elastic behavior of enamel supported by dentin.

Hertzian characterization of the tooth, using load rate as an independent variable, led to the discovery of visco-elastic properties of enamel supported by dentin. These properties were manifested in an inverse relationship between the extent of damage produced and load rate applied (i.e. as load rate increased observed damage decreased). At a high load rate (i.e. 144 N/min), elastic behavior, rather than brittle or quasi-plastic, was dominant. Clinically, this can be justified by the tooth's observed tolerance of millions of cycles of high loads at very high loading rates (i.e. >600 N/min).

The Hertzian characterization of the tooth as a bi-layer structure should be extended. More definitive characterization will need to begin by increasing sample size. This will allow for statistical analysis that can overcome the problems presented by biologic variability. Hertzian contact testing will need to be performed at a number of given loads varying only load rate. Loads and load rates chosen should be clinically relevant to those observed under functional loading at both low and high extremes. Increments of load rate should be relatively small for interpolation of the onset of the apparent visco-elastic properties exhibited by the tooth in this thesis. An investigation of the effect of ranges of indenter size should also be performed relative to the damage modes produced.

Once the load rate that induces elastic behavior is determined, tests should be performed at varying loads above that load rate. This will allow for determination of critical loads to induce other brittle and quasi-plastic damage. Once this critical load is determined, tests can be performed to determine critical values at other load rates.

These studies will allow for further insight into the tooth's remarkable accommodation and tolerance of contacts under functional loading. Insight may be

gained into the evolution of tooth microstructure relative to functional demands. Once the tooth is and its inherent properties are better understood, the emergence of a new class of bio-mimetic dental materials and restorations that will mimic the tooth, not only in form and function, but performance as well, can be witnessed.

APEENDIX

ADDITIONAL DATA AND FIGURES

This appendix provides supplemental results referred to in Chapter 4.

Table A.1 Raw data for all specimens successfully tested.

LOAD RATE (N/min)	LOAD (N)	ENAMEL THICKNESS (mm)	CONTACT RADIUS (mm)	INDENTATION STRESS (MPa)	INDENTATION STRAIN	RELATIVE ELASTIC MODULUS (MPa)
18	~50	0.25	0.525	58	0.33	176
18	~50	0.5	0.5	64	0.32	200
18	~50	0.75	0.475	71	0.3	237
18	~50	1.05	0.45	79	0.28	282
18	~75	0.4	0.5	95.8	0.316	303
18	~75	0.45	0.5	96	0.316	304
18	~75	0.95	0.425	133	0.269	404
18	~75	1.3	0.375	170	0.237	717
144	~100	0.3	0.25	518	0.158	3278
144	~100	0.5	0.225	636	0.142	4479
144	~100	0.9	0.3	359	0.19	1889
144	~100	0.95	0.25	518	0.158	3278
144	~100	1.1	0.25	518	0.158	3278
144	~100	1.25	0.125	2066	0.079	26152
144	~150	0.3	0.25	774	0.158	4899
144	~150	0.35	0.275	638	0.174	3667
144	~150	0.55	0.275	638	0.174	3667
144	~150	1.4	0.3	536	0.19	2821

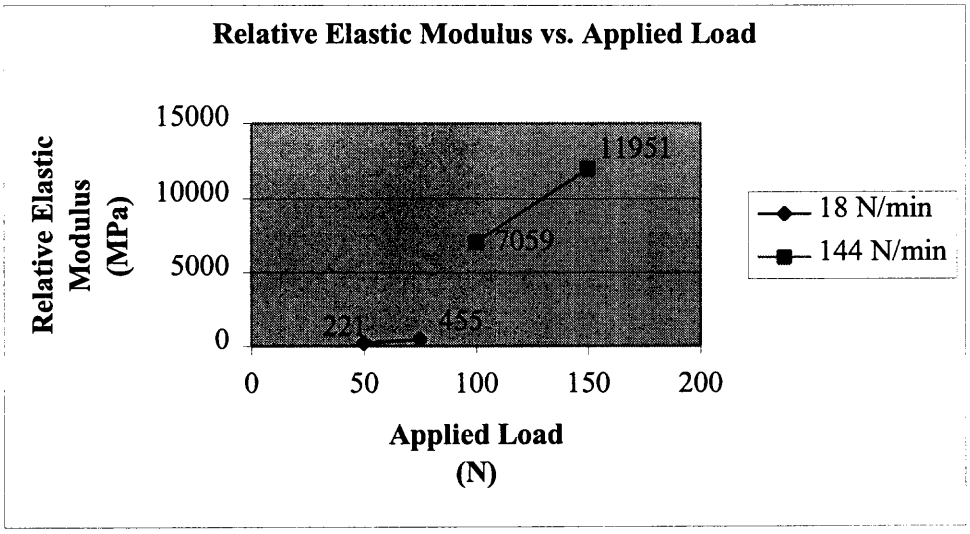

Figure A.1 Plot of Relative Elastic Modulus vs. Applied Load among groups.

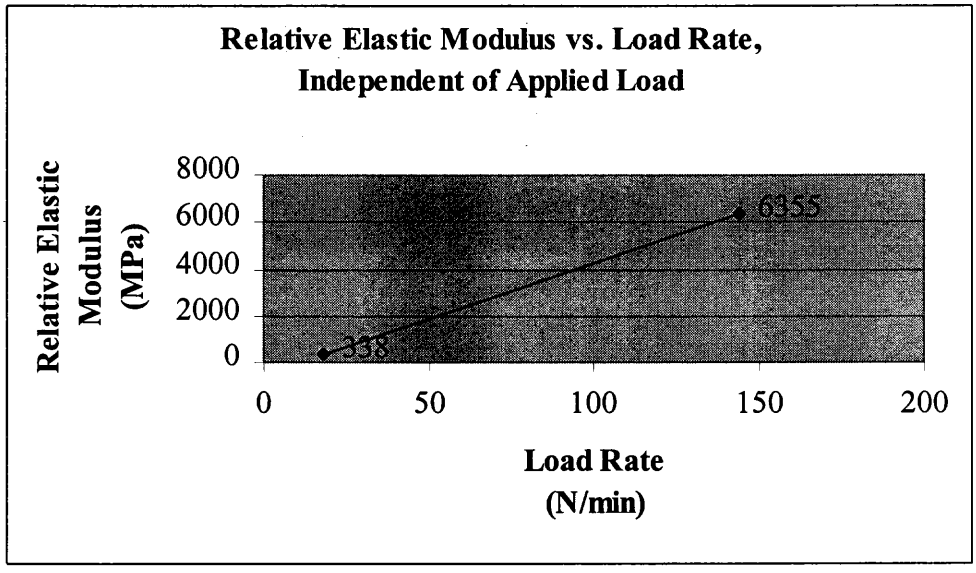

Figure A.2 Plot of Relative Elastic Modulus vs. Load Rate, Independent of Applied Load among groups.

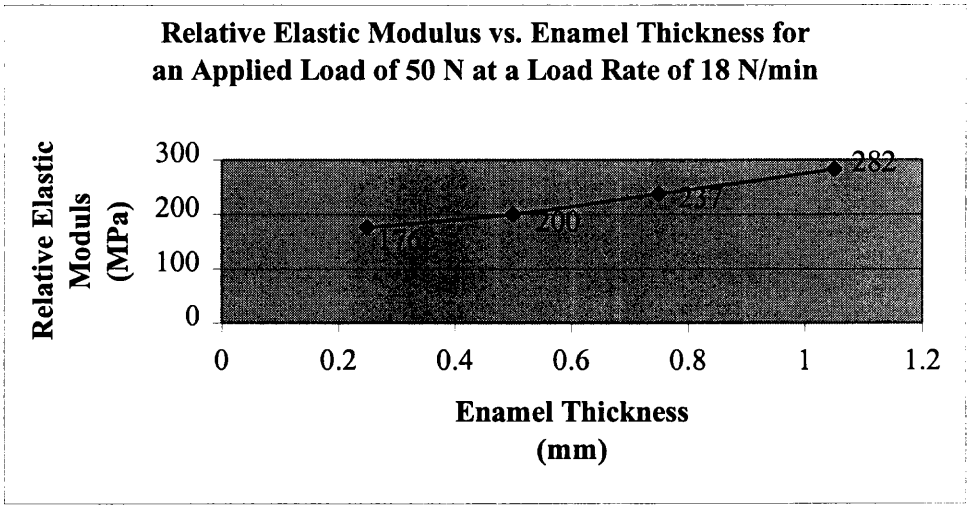

Figure A.3 Plot of Relative Elastic Modulus vs. Enamel Thickness for an Applied Load of 50 N at a Load Rate of 18 N/min.

Table A.2 Data set for specimens tested to a load of 75 N at a rate of 18 N/min.

Applied Load (N)	Load Rate (N/min)	Enamel Thickness (mm)	Contact Radius (mm)	Indentation Stress (MPa)	Indenation Strain	Relative Elastic Modulus (MPa)
75	18	0.4	0.5	95.8	0.316	303
75	18	0.45	0.5	96	0.316	304
75	18	0.95	0.425	133	0.269	494
75	18	1.3	0.375	170	0.237	717

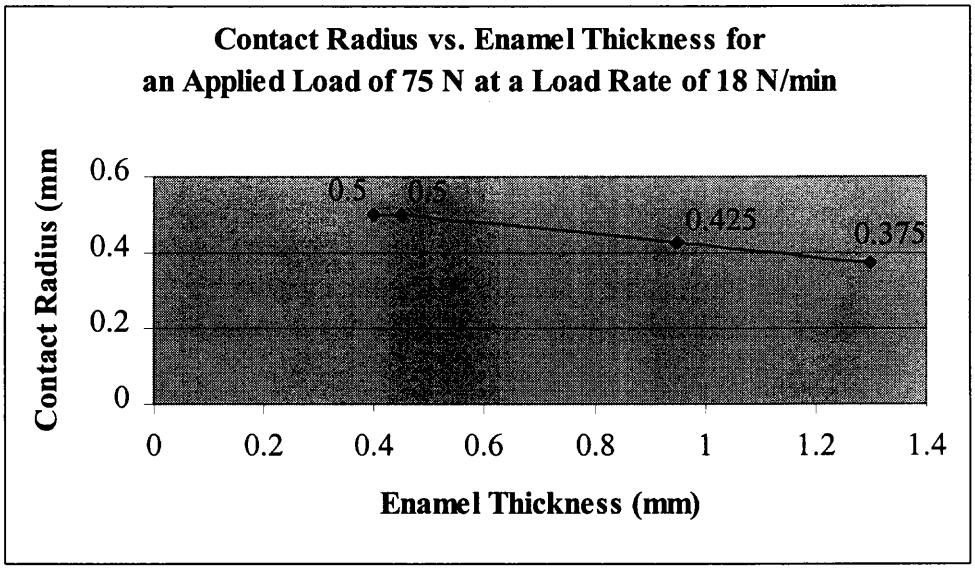

Figure A.4 Plot of Contact Radius vs. Enamel Thickness for an Applied Load of 75 N at a Load Rate of 18 N/min.

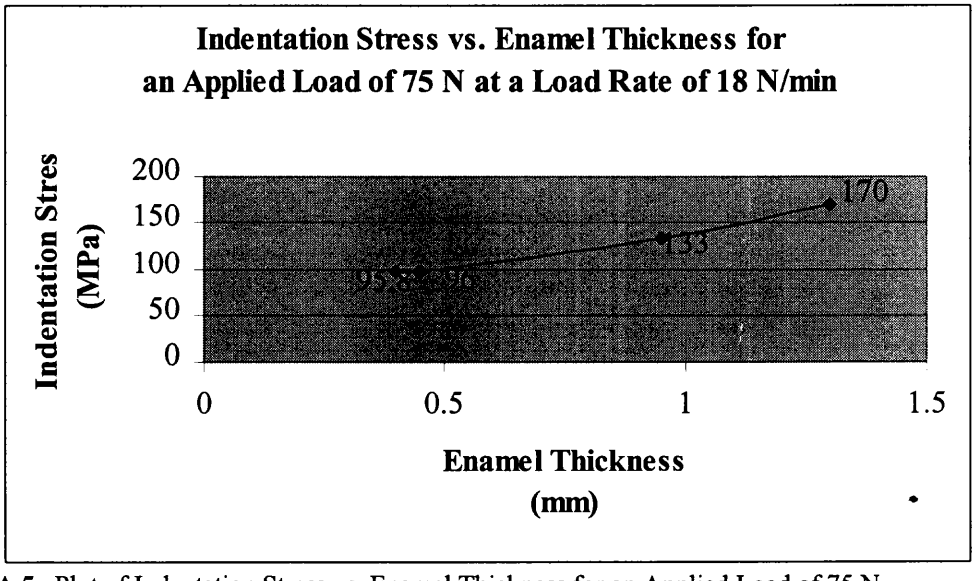

Figure A.5 Plot of Indentation Stress vs. Enamel Thickness for an Applied Load of 75 N at a Load Rate of 18 N/min.

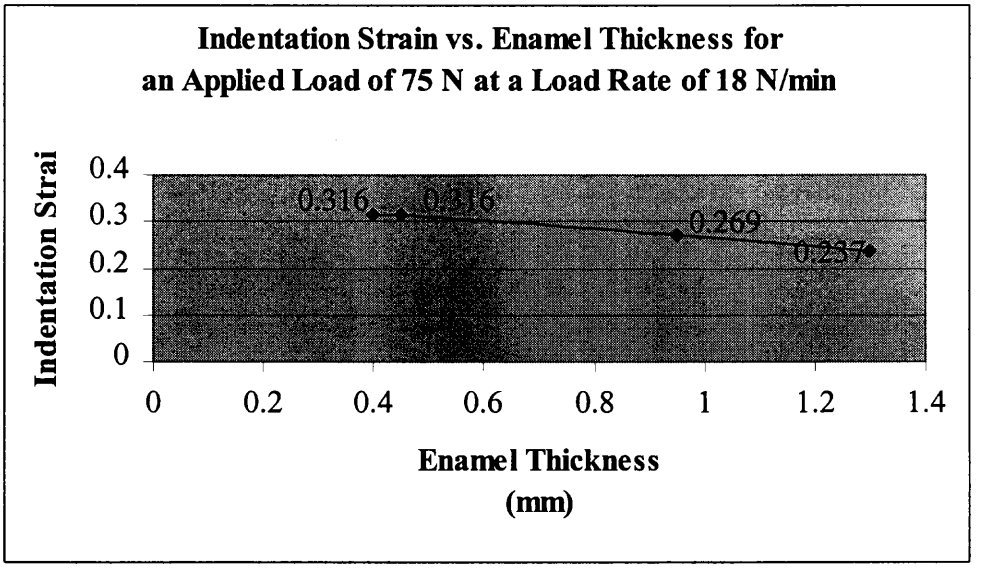

Figure A.6 Plot of Indentation Strain vs. Enamel Thickness for an Applied Load of 75 N at a Load Rate of 18 N/min.

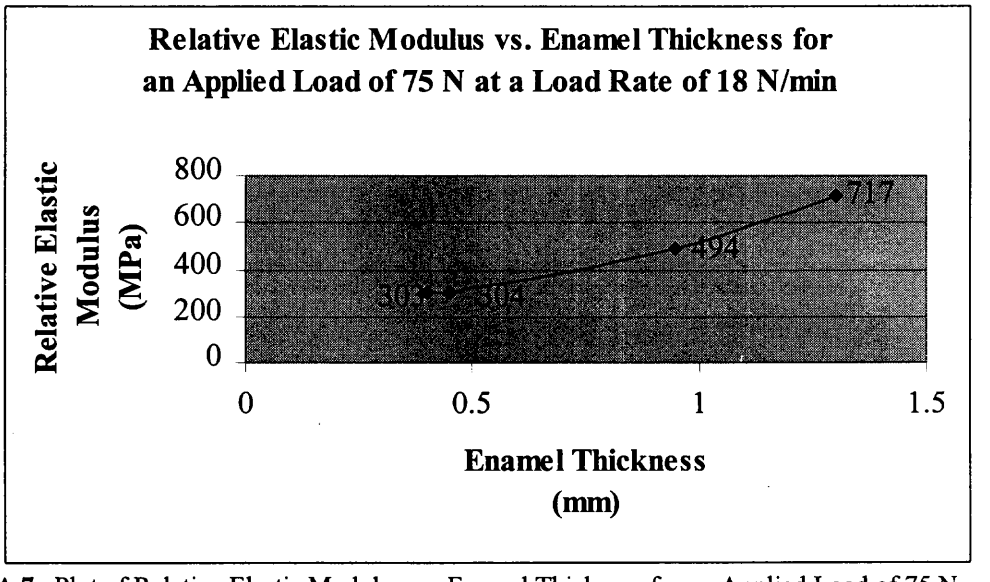

Figure A.7 Plot of Relative Elastic Modulus vs. Enamel Thickness for an Applied Load of 75 N at a Load Rate of 18 N/min.

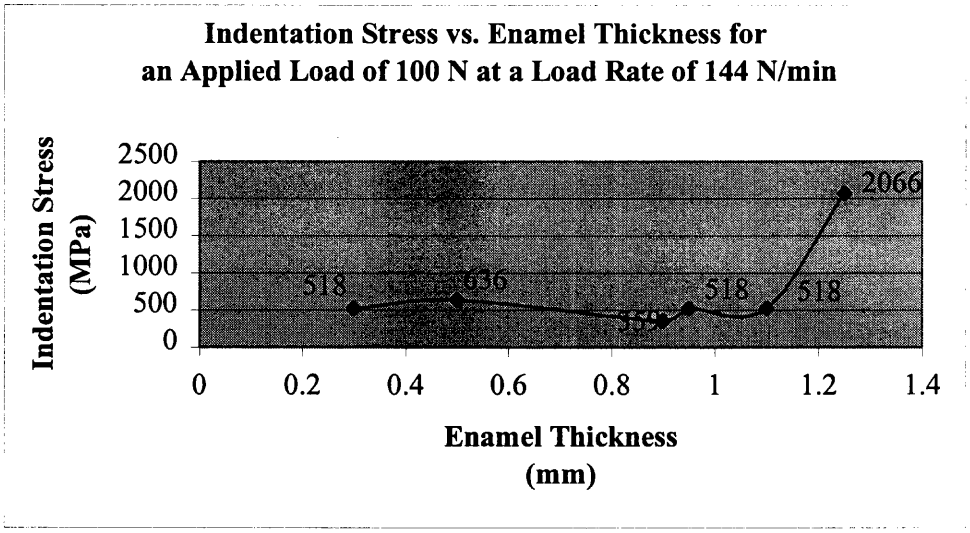

Figure A.8 Plot of Indentation Stress vs. Enamel Thickness for an Applied Load of 100 N at a Load Rate of 144 N/min.

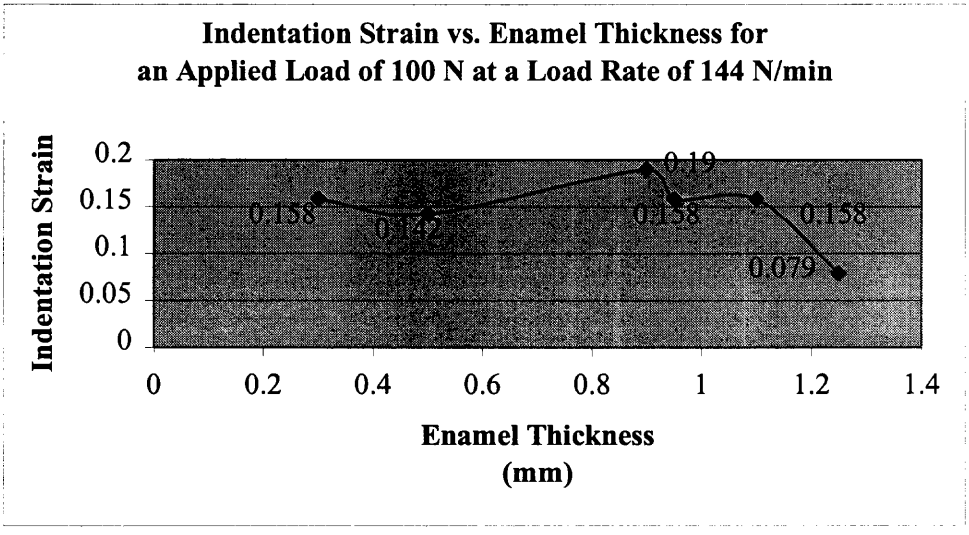

Figure A.9 Plot of Indentation Strain vs. Enamel Thickness for an Applied Load of 100 N at a Load Rate of 144 N/min.

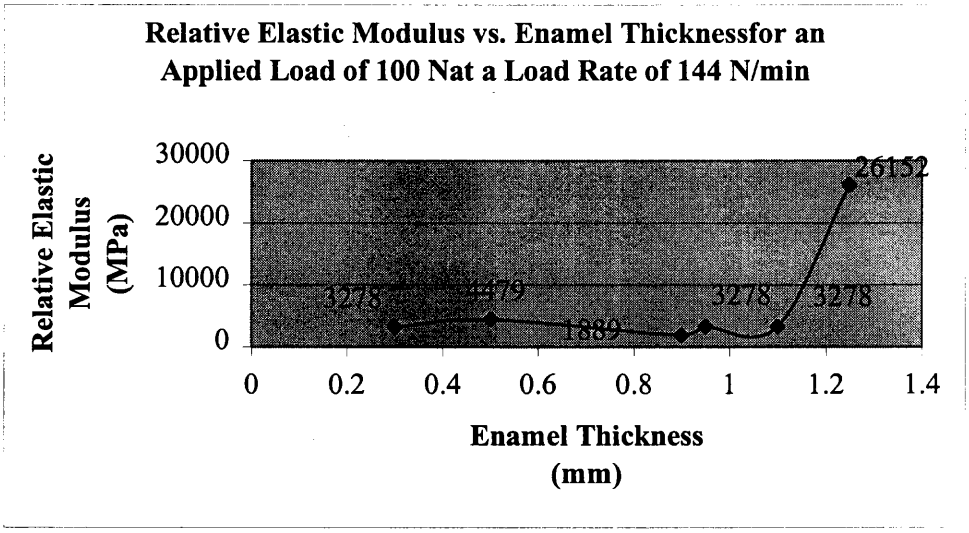

Figure A.10 Plot of Relative Elastic Modulus vs. Enamel Thickness for an Applied Load of 100 N at a Load Rate of 144 N/min.

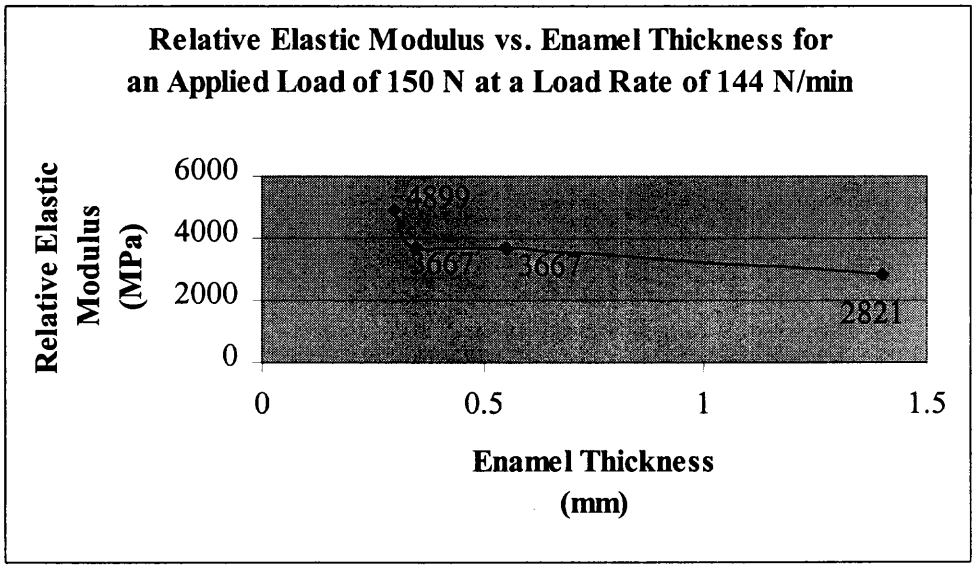

Figure A.11 Plot of Relative Elastic Modulus vs. Enamel Thickness for an Applied Load of 150 N at a Load Rate of 144 N/min.

REFERENCES

1. Rekow, E.D., *Project 4: characterization of the dental substrate for bio-mimetic design.*, UMDNJ - Dental School: Newark. p. 174-192.

2. Lawn, B.R., *All-ceramic crown-like layer structures: characterization and design.* J Prosthet Dent, 2001, in press.

3. Wuttiphan, S., *Contact Damage and Fracture of Ceramic Layer Structures*, in *Department of Materials and Nuclear Engineering.* 1997, University of Maryland. p. 157.

4. Kelly, J.R., *Clinically relevant approach to failure testing of all-ceramic restorations.* J Prosthet Dent, 1999. 81(6): p. 652-61.

5. Jung, Y.G., et al., *Damage modes in dental layer structures.* J Dent Res, 1999. 78(4): p. 887-97.

6. Ten Cate, A.R., *Structure of the oral tissues*, in *Oral Histology: Development, Structure, and Function.* 1989, C.V. Mosby Company: St. Louis. p. 44-9.

7. Lundeen, T.F., Sturdevant, J.R. and Sluder, T.B. Jr, *Clinical significance of dental anatomy, histology, physiology, and occlusion*, in *The Art and Science of Operative Dentistry*, C.M. Sturdevant, Editor. 1995, Mosby: St. Louis. p. 10-57.

8. Eisenmann, D.R., *Enamel Structure*, in *Oral Histology: Development, Structure, and Function.* 1989, C.V. Mosby Company: St. Louis. p. 213-28.

9. Waters, N.E., *Some mechanical and physical properties of teeth.* Symp Soc Exp Biol, 1980. 34: p. 99-135.

10. Osborn, J.W., *Directions and interrelationships of enamel prisms from the sides of human teeth.* J Dent Res, 1968. 47(2): p. 223-32.

11. Hirota, F., *Prism arrangement in human cusp enamel deduced by X-ray diffraction.* Arch Oral Biol, 1982. 27(11): p. 931-7.

12. Applebaum, E., *The arrangement of enamel rods.* NY State Dental Journal, 1960. 26: p. 185-188.

13. Torneck, C.D., *Dentin-Pulp Complex*, in *Oral Histology: Development, Structure, and Function.* 1989, C.V. Mosby Company: St. Louis. p. 157-77.

14. Rasmussen, S.T., *Fracture properties of human teeth in proximity to the dentinoenamel junction.* J Dent Res, 1984. 63(11): p. 1279-83.

15. Lin, C.P., W.H. Douglas, and S.L. Erlandsen, *Scanning electron microscopy of type I collagen at the dentin-enamel junction of human teeth.* J Histochem Cytochem, 1993. 41(3): p. 381-8.

16. Marshall, G.W., et al., *Mechanical properties of the dentinoenamel junction: AFM studies of nanohardness, elastic modulus, and fracture.* J Biomed Mater Res, 2001. 54(1): p. 87-95.

17. Craig, R.G., *Elastic and mechanical properties of human dentin.* J Dent Res, 1958. 37(4): p. 710-718.

18. Craig, R.G., *Compressive properties of enamel, dental cements, and gold.* J Dent Res, 1961. 40: p. 936-943.

19. Willems, G., et al., *Hardness and Young's modulus determined by nanoindentation technique of filler particles of dental restorative materials compared with human enamel.* J Biomed Mater Res, 1993. 27(6): p. 747-55.

20. Xu, H.H., et al., *Indentation damage and mechanical properties of human enamel and dentin.* J Dent Res, 1998. 77(3): p. 472-80.

21. Rasmussen, S.T., et al., *Fracture properties of human enamel and dentin.* J Dent Res, 1976. 55(1): p. 154-64.

22. Rasmussen, S.T. and R.E. Patchin, *Fracture properties of human enamel and dentin in an aqueous environment.* J Dent Res, 1984. 63(12): p. 1362-8.

23. Lin, C.P. and W.H. Douglas, *Structure-property relations and crack resistance at the bovine dentin- enamel junction.* J Dent Res, 1994. 73(5): p. 1072-8.

24. Lawn, B.R., *Fracture of brittle solids.*. 1993, Cambridge University Press: Cambridge. p. 55.

25. Hassan, R., A.A. Caputo, and R.F. Bunshah, *Fracture toughness of human enamel.* J Dent Res, 1981. 60(4): p. 820-7.

26. Van Meerbeek, B., et al., *Assessment by nano-indentation of the hardness and elasticity of the resin-dentin bonding area.* J Dent Res, 1993. 72(10): p. 1434-42.

27. Spears, I.R., et al., *The effects of enamel anisotropy on the distribution of stress in a tooth.* J Dent Res, 1993. 72(11): p. 1526-31.

28. Goel, V.K., S.C. Khera, and K. Singh, *Clinical implications of the response of enamel and dentin to masticatory loads.* J Prosthet Dent, 1990. 64(4): p. 446-54.

29. Caputo, A.a.W., R., *Force Generation and Reaction Within the Periodontium.*

30. Hertz, H., *Hertz's Miscellaneous Papers.* 1896, London, Chs. 5,6: Macmillan.

31. Johnson, K.L., *Contact Mechanics.* 1985, London: Cambridge University Press.

32. Lawn, B.R., Wilshaw, T.R., *Indentation Fracture: Principles and Applications.* Journal of Material Science, 1975. 10(6): p. 1049-81.

33. Guiberteau, F.e.a., *Effect of Grain Size on Hertzian Contact in Alumina.* J Am Ceram Soc, 1994. 77(7): p. 1825-31.

34. Peterson, I.M., et al., *Mechanical characterization of dental ceramics by hertzian contacts.* J Dent Res, 1998. 77(4): p. 589-602.

35. Guiberteau, F.e.a., *Indentation fatigue: a simple cyclic Hertzian test for measuring damage accumulation in polycrystallin ceramics.*, in *Phil Mag.* 1993. p. 1003-1016.

36. Roesler, F.C., *Brittle Fractures Near Equilibrium.* Proc Phys Soc London, 1956. B69: p. 981.

37. Frank, F.C., Lawn B.R., *On the Theory of Hertzian Fracture.* Proc R Soc London, 1967. A299(458): p. 291-306.

38. Lawn, B.R., Padture, N.P., Chai, H. and Guiberteau, F., *Making Ceramics Ductile.* Science, 1994. 263: p. 1114-16.

39. Padture, N.P.a.L., B.R., *Fatigue in Ceramics with Interconnecting Weak Interfaces: A Study Using Cyclic Hertzian Contacts.* Acta Metallurgica, 1995. 43(4): p. 1609-17.

40. Jaeger, J.C.a.C., N.G.W., *Fundamentals of Rock Mechanics.* 1971, London: Chapman and Hall.

41. Horri, H.a.N.-N., S., *Compression-Induced Microcrack Growth in Brittle Solids: Axial Splitting and Shear Failure.* J Geophys Res, 1985. 90(B4): p. 3105-25.

42. Ashby, M.F.a.H., S.D., *The Failure of Brittle Solids Containing Small Cracks Under Compressive Stress States.* Acta Metallurgica et Materialia, 1986. 34(3): p. 497-510.

43. Chai, H., Stevens KAlceff, M.A. and Lawn, B.R., *Deformation and Fracture of Mica-Containing Glass-Ceramics in Hertzian Contacts.* j mater res, 1994. 9(3): p. 762-70.

44. Padture, N.P.a.L., B.R., *Toughness properties of a cilicon carbide with an in-citu-Induced heterogeneous grain structure.* J Am Ceram Soc, 1994. 77(10): p. 2518-22.

45. Xu, H.H., Wei, L., Padture, N.P., Lawn, B.R. and Yeckly, R.L., *Effect of Microstructural Coarsening on Hertzian Contact Damage in Silicon Nitride.* J Mater Sci, 1995. 30: p. 869-78.

46. Padture, N.P.a.L., B.R., *Contact Fatigue of a Silicon Carbide With a Heterogeneous Grain Structure.* J Am Ceram Soc, 1995. 78(6): p. 1431-38.

47. An, L., Chan, H.M., Padture, N.P., and Lawn, B.R., *Damage-Resistant Alumina Based Layer Composites.* j mater res, 1996. 11(1): p. 204-10.

48. Wuttiphan, S., Lawn, B.R., and Padture, N.P., *Crack Suppression in Strongly-Bonded Homogeneous/Heterogeneous Laminates: A Study on Glass/Glass-Ceramic Bi-Layers.* J Am Ceram Soc, 1996. 79(3): p. 634-640.

49. Lee, S.K., S. Wuttiphan, and B.R. Lawn, *Role of Microstructure in Hertzian Contact Damage in Silicon Nitride: I. Mechanical Characterization.* Journal of the American Ceramic Society, 1997. in press.

50. Lawn, B.R., *Indentation of Ceramics with Spheres: A Century after Hertz.* J Am Ceram Soc, 1998. 81(8): p. 1977-94.

51. Peterson, I.M., et al., *Role of microstructure on contact damage and strength degradation of micaceous glass-ceramics.* Dent Mater, 1998. 14(1): p. 80-9.

52. Rhee, Y., Kim, H., Deng, Y. and Lawn, B.R., *Brittle fracture versus quasi plasticity in ceramics: a simple predictive index.* J Am Ceram Soc, 2001. 84(3): p. 561-65.

53. Chai, H., Lawn, B.R. and Wuttiphan, S., *Fracture Modes in Brittle Coatings with Large interlayer modulus mismatch.* J Mater Res, 1999. 14(9): p. 3805-17.

54. Lee, S.K., Wuttiphan, S., Hu, X., Lee, S.K. and Lawn, B.R., *Contact-induced transverse fractures in brittle layers on soft substrates: a study on silicon nitride bilayers.* J Am Ceram Soc, 1998. 81(3): p. 571-80.

55. Begley, M.R., Evans, A.G. and Hutchinson, J.W., Int J Solids Struct, 1999. 36: p. 2773.

56. Warshawsky, H., *Organization of crystals in enamel.* Anatom. Rec., 1989. 224: p. 242-62.

57. Weber, D.E., *Sheath configurations in human cuspal enamel.* J Morphol., 1975. 141(479-87).

58. Habelitz, S., et al., *Mechanical properties of human dental enamel on the nanometer scale.* Arch Oral Biol, 2001. 46(2): p. 173-83.

59. Balooch, M., et al., *Viscoelastic properties of demineralized human dentin measured in water with atomic force microscope (AFM)-based indentation.* J Biomed Mater Res, 1998. 40(4): p. 539-44.